in WHHLMI rabbits that developed various atherosclerotic changes, early to advanced lesions, in the same individual. Consequently, we found that the LOX-1 expression was the highest in the atheromatous lesions (type IV) (Fig. 4B), which could mainly be caused by extensive LOX-1 expression in macrophages-rich area (Fig. 1R, 5II left). The current results support our earlier study where we showed a correlation between LOX-1 expression and morphological plaque instability.[16] In addition, Kataoka *et al.* reported LOX-1 expression in macrophages and smooth muscle cells in human advanced atherosclerotic lesions.[24] On the other hand, Chen *et al.* reported that LOX-1 expression was observed in endothelial cells, macrophages and smooth muscle cells in early atherosclerotic lesions.[25] The moderate LOX-1 expression in the neointimal lesions observed in our rabbits was consistent with the results reported by Chen *et al.*

TF has been known as an initiating factor in the coagulation protease cascade. TF expression has been suggested by several studies to be linked with thrombus formation after the plaque rupture. TF expression has been detected within the macrophage-rich areas, but is absent in the fibrous tissue.[26,27] Concordantly, TF expression was extensively shown in the lipid area (Fig. 5II right) of atheromatous lesions (Fig. 4C) in the present study. The spatial distribution of TF and LOX-1 immunostaining in serial sections suggests the colocalization of these antigens in RAM-11-positive macrophage-rich area (Figs. 1, 3A—C, 5). In addition, the TF expression was positively correlated with the LOX-1 expression in the atherosclerotic plaques (Fig. 6D). Thus, our data provide *in vivo* evidence for the correlated expression between LOX-1 and TF. These findings appear to suggest that LOX-1 may be involved in Ox-LDL-induced TF expression in the lipid rich plaques *in vivo*. The CD40/CD40L signaling pathway may be involved in this process, since Ox-LDL-LOX-1 interactions activate the CD40/CD40L signaling pathway,[13,14] which thereby induces TF expression.[15] Thus, LOX-1 may play a key role in TF expression, and thereby thrombus formation *in vivo*. In addition, previous *in vitro* studies have also reported that expression of TF and LOX-1 are mediated by nuclear factor-κB (NF-κB) activation.[28—30] The proinflammatory transcription factor, NF-κB, has been known to mediate transcription of a wide variety of genes induced by proinflammatory simuli, including IL-1α, IL-1β, TNF-α, and Ox-LDL.[31] Therefore, coordinated expression of TF and LOX-1 in the macrophage-rich lipid area of the atheromatous lesions may be regulated by NF-κB.

Apoptosis is one of the causative factors in the formation of vulnerable atherosclerotic plaques. Apoptosis of foam cells and macrophages is thought to promote plaque vulnerability by causing the accumulation of an acellular (cell-poor) lipid core.[4] In the present study, LOX-1 expression was prominent in the macrophage-rich lipid area where TUNEL-positive cells were mainly observed (Figs. 3A—D). When quantified by histomorphometry, the significant correlation between LOX-1 expression and apoptotic events in the atherosclerotic lesions was observed (Fig. 6E). On the other hand, the translocation of phosphatidylserine to the cell surface that occurred during apoptotic cell death was reportedly correlated to a high TF expression.[26,32] Concordantly, we detected marked TF expression in close proximity to apoptotic foam cells within the macrophage-rich lipid area (Figs. 3C, D). Taken together, a potential *in vivo* interaction among LOX-1, TF and apoptotic events may be proposed. LOX-1 may promote TF expression not only *via* the CD40/CD40L signaling pathway, but also the apoptosis of foam cells in the macrophage-rich lipid area of atheromatous lesions. Further studies on the LOX-1-dependent activation of caspase-9 and caspase-3, and/or the regulation of Bcl-2 and c-IAP-1[11] would clarify the potential linkage.

It is also reported that the apoptosis of smooth muscle cells could weaken the fibrous cap *via* a decrease in the synthesis of the extracellular matrix.[5] Previous studies suggested that LOX-1 expression may also play a role in the development of apoptosis in smooth muscle cells.[10,11,24] In the present study, however, TUNEL-positive nuclei were mainly observed in macrophage-rich lipid area where LOX-1 expression is abundant using a rabbit hyperlipidemic model. Several previous studies have indicated that Ox-LDL-LOX-1 interaction in macrophages promotes MMPs involved in the degradation of extracellular matrix proteins,[12] which is consistent with our current and previous results in WHHLMI rabbits.[16]

It is of great importance to discuss the animal model used in the present study (WHHLMI rabbits). Unfortunately, animal models suitable for studying the spontaneous rupture of unstable plaques have yet to be established. However, it has been reported that hemorrhage, plaque rupture and thrombosis (type VI) are occasionally observed in coronary lesions of WHHLMI rabbits, although the atherosclerotic plaques are not prone to rupture.[33] In fact, the pathological features of atheromatous lesions observed in our rabbits were similar to those of human unstable plaques.[17,18,34,35] Thus, the use of WHHLMI rabbits could be effective for investigating causative factors in the destabilization of atherosclerotic plaques and help translate laboratory observations to the clinical setting.

CONCLUSION

The present data from the atherosclerotic specimens of WHHLMI rabbits demonstrate a pathobiological link among LOX-1, TF, apoptotic events and the vulnerability of atherosclerotic plaques, suggesting that the vulnerability and thrombotic activity of atherosclerotic lesions may result from a LOX-1 signal linkage. The present findings should help understand the pathophysiology of atherosclerosis, leading to the development of new therapeutic and diagnostic (imaging) agents of atherosclerosis.

Acknowledgements This work was partly supported by a Grant-in-Aid for General Scientific Research from the Ministry of Education, Culture, Sports, Science and Technology of Japan, and from the Japan Society for the Promotion of Science, by a research grant from New Energy and Industrial Technology Development Organization (NEDO), by a research grant for Cardiovascular diseases from the Ministry of Health, Labor and Welfare (16C-8) and by the 21st Century COE Program, 'Knowledge Information Infrastructure for Genome Science.'

REFERENCES

1) Ruberg F. L., Leopold J. A., Loscalzo J., *Prog. Cardiovasc. Dis.*, **44**, 381—394 (2002).
2) Falk E., Shah P. K., Fuster V., *Circulation*, **92**, 657—671 (1995).
3) Moons A. H., Levi M., Peters R. J., *Cardiovasc. Res.*, **53**, 313—325 (2002).
4) Bjorkerud S., Bjorkerud B., *Am. J. Pathol.*, **149**, 367—380 (1996).
5) Geng Y. J., Henderson L. E., Levesque E. B., Muszynski M., Libby P., *Arterioscler. Thromb. Vasc. Biol.*, **17**, 2200—2208 (1997).
6) Sawamura T., Kume N., Aoyama T., Moriwaki H., Hoshikawa H., Aiba Y., Tanaka T., Miwa S., Katsura Y., Kita T., Masaki T., *Nature* (London), **386**, 73—77 (1997).
7) Li D., Mehta J. L., *Circulation*, **101**, 2889—2895 (2000).
8) Moriwaki H., Kume N., Kataoka H., Murase T., Nishi E., Sawamura T., Masaki T., Kita T., *FEBS Lett.*, **440**, 29—32 (1998).
9) Smirnova I. V., Kajstura M., Sawamura T., Goligorsky M. S., *Am. J. Physiol. Heart Circ. Physiol.*, **287**, 782—790 (2004).
10) Kataoka H., Kume N., Miyamoto S., Minami M., Morimoto M., Hayashida K., Hashimoto N., Kita T., *Arterioscler. Thromb. Vasc. Biol.*, **21**, 955—960 (2001).
11) Kume N., Kita T., *Circ. Res.*, **94**, 269—270 (2004).
12) Li D., Liu L., Chen H., Sawamura T., Ranganathan S., Mehta J. L., *Circulation*, **107**, 612—617 (2003).
13) Li D., Liu L., Chen H., Sawamura T., Mehta J. L., *Arterioscler. Thromb. Vasc. Biol.*, **23**, 816—821 (2003).
14) Schonbeck U., Libby P., *Circ. Res.*, **89**, 1092—1103 (2001).
15) Sanguigni V., Ferro D., Pignatelli P., Del Ben M., Nadia T., Saliola M., Sorge R., Violi F., *J. Am. Coll. Cardiol.*, **45**, 35—42 (2005).
16) Ishino S., Mukai T., Kume N., Asano D., Ogawa M., Kuge Y., Minami M., Kita T., Shiomi M., Saji H., *Atherosclerosis*, **195**, 48—56 (2007).
17) Shiomi M., Ito T., Tsukada T., Yata T., Ueda M., *Arterioscler. Thromb.*, **14**, 931—937 (1994).
18) Shiomi M., Ito T., Yamada S., Kawashima S., Fan J., *Arterioscler. Thromb. Vasc. Biol.*, **23**, 1239—1244 (2003).
19) Ishino S., Kuge Y., Takai N., Tamaki N., Strauss H. W., Blankenberg F. G., Shiomi M., Saji H., *Eur. J. Nucl. Med. Mol. Imaging*, **34**, 889—899 (2007).
20) Stary H. C., Chandler A. B., Glagov S., Guyton J. R., Insull W. Jr., Rosenfeld M. E., Schaffer S. A., Schwartz C. J., Wagner W. D., Wissler R. W., *Circulation*, **89**, 2462—2478 (1994).
21) Stary H. C., Chandler A. B., Dinsmore R. E., Fuster V., Glagov S., Insull W. Jr., Rosenfeld M. E., Schwartz C. J., Wagner W. D., Wissler R. W., *Circulation*, **92**, 1355—1374 (1995).
22) Shiomi M., Ito T., Hirouchi Y., Enomoto M., *Ann. N. Y. Acad. Sci.*, **947**, 419—423 (2001).
23) Shiomi M., Ito T., Hirouchi Y., Enomoto M., *Atherosclerosis*, **157**, 75—84 (2001).
24) Kataoka H., Kume N., Miyamoto S., Minami M., Moriwaki H., Murase T., Sawamura T., Masaki T., Hashimoto N., Kita T., *Circulation*, **99**, 3110—3117 (1999).
25) Chen M., Kakutani M., Minami M., Kataoka H., Kume N., Narumiya S., Kita T., Masaki T., Sawamura T., *Arterioscler. Thromb. Vasc. Biol.*, **20**, 1107—1115 (2000).
26) Hutter R., Valdiviezo C., Sauter B. V., Savontaus M., Chereshnev I., Carrick F. E., Bauriedel G., Lüderitz B., Fallon J. T., Fuster V., Badimon J. J., *Circulation*, **109**, 2001—2008 (2004).
27) Aikawa M., Rabkin E., Sugiyama S., Voglic S. J., Fukumoto Y., Furukawa Y., Shiomi M., Schoen F. J., Libby P., *Circulation*, **103**, 276—283 (2001).
28) Hofnagel O., Luechtenborg B., Eschert H., Weissen-Plenz G., Severs N. J., Robenek H., *Arterioscler. Thromb. Vasc. Biol.*, **26**, 604—610 (2006).
29) Armstead V. E., Opentanova I. L., Minchenko A. G., Lefer A. M., *Anesthesiology*, **91**, 1844—1852 (1999).
30) Parry G. C., Mackman N., *Arterioscler. Thromb. Vasc. Biol.*, **15**, 612—621 (1995).
31) Ghosh S., May M. J., Kopp E. B., *Ann. Rev. Immunol.*, **16**, 225—260 (1998).
32) Mallat Z., Hugel B., Ohan J., Leseche G., Freyssinet J. M., Tedgui A., *Circulation*, **99**, 348—353 (1999).
33) Shiomi M., Ito T., Yamada S., Kawashima S., Fan J., *J. Atheroscler. Thromb.*, **11**, 184—189 (2004).
34) Kolodgie F. D., Burke A. P., Farb A., Gold H. K., Yuan J., Narula J., Finn A. V., Virmani R., *Curr. Opin. Cardiol.*, **16**, 285—292 (2001).
35) Kullo I. J., Edwards W. D., Schwartz R. S., *Ann. Intern. Med.*, **129**, 1050—1060 (1998).

Targeting of Lectinlike Oxidized Low-Density Lipoprotein Receptor 1 (LOX-1) with ^{99m}Tc-Labeled Anti–LOX-1 Antibody: Potential Agent for Imaging of Vulnerable Plaque

Seigo Ishino[1], Takahiro Mukai[2], Yuji Kuge[1], Noriaki Kume[3], Mikako Ogawa[4], Nozomi Takai[1], Junko Kamihashi[1], Masashi Shiomi[5], Manabu Minami[3], Toru Kita[3], and Hideo Saji[1]

[1]Department of Patho-Functional Bioanalysis, Graduate School of Pharmaceutical Sciences, Kyoto University, Kyoto, Japan; [2]Department of Biomolecular Recognition Chemistry, Graduate School of Pharmaceutical Sciences, Kyushu University, Fukuoka, Japan; [3]Department of Cardiovascular Medicine, Graduate School of Medicine, Kyoto University, Kyoto, Japan; [4]Laboratory of Genome Bio-Photonics Photon Medical Research Center, Hamamatsu University School of Medicine, Hamamatsu, Japan; and [5]Institute for Experimental Animals, Kobe University School of Medicine, Kobe, Japan

Lectinlike oxidized low-density lipoprotein (LDL) receptor 1 (LOX-1), a cell surface receptor for oxidized LDL, has been implicated in vascular cell dysfunction related to plaque instability, which could be a potential target for an atherosclerosis imaging tracer. In this study, we designed and prepared ^{99m}Tc-labeled anti–LOX-1 monoclonal IgG and investigated its usefulness as an atherosclerosis imaging agent. **Methods:** Anti–LOX-1 monoclonal IgG and control mouse IgG2a were labeled with ^{99m}Tc after derivatization with 6-hydrazinonicotinic acid to yield ^{99m}Tc-LOX-1-mAb and ^{99m}Tc-IgG2a, respectively. Myocardial infarction–prone Watanabe heritable hyperlipidemic (WHHLMI) rabbits (atherosclerosis model) and control rabbits were injected intravenously with these probes, and in vivo planar imaging was performed. At 24 h after the injection, the aortas were removed, and radioactivity was measured. Autoradiography and histologic studies were performed with serial aortic sections. **Results:** The level of ^{99m}Tc-LOX-1-mAb accumulation was 2.0-fold higher than the level of ^{99m}Tc-IgG2a accumulation in WHHLMI rabbit aortas, and the level of ^{99m}Tc-LOX-1-mAb accumulation in WHHLMI rabbit aortas was 10.0-fold higher than the level of ^{99m}Tc-LOX-1-mAb accumulation in control rabbit aortas. In vivo imaging clearly visualized the atherosclerotic aortas of WHHLMI rabbits. Autoradiography and histologic studies revealed that regional ^{99m}Tc-IgG2a accumulation was independent of the histologic grade of the lesions; however, regional ^{99m}Tc-LOX-1-mAb accumulation was significantly correlated with LOX-1 expression density and the vulnerability index. The highest level of ^{99m}Tc-LOX-1-mAb accumulation, expressed as {radioactivity in region of interest (Bq/mm^2)/[injected radioactivity (Bq)/animal body weight (g)]} × 10^2, was found in atheromatous lesions (3.8 ± 1.1 [mean ± SD]), followed in decreasing order by fibroatheromatous lesions (2.0 ± 1.0), collagen-rich lesions (1.6 ± 0.8), and neointimal lesions (1.4 ± 0.7). **Conclusion:** The level of ^{99m}Tc-LOX-1-mAb accumulation in grade IV atheroma was higher than that in neointimal lesions or other, more stable lesions. Nuclear imaging of LOX-1 expression with ^{99m}Tc-LOX-1-mAb may be a useful means for predicting atheroma at high risk for rupture.

Key Words: plaque; receptor; antibody; imaging; atherosclerosis

J Nucl Med 2008; 49:1677–1685
DOI: 10.2967/jnumed.107.049536

The spontaneous rupture of vulnerable atherosclerotic plaques and subsequent thrombus formation are currently recognized as the primary mechanisms of myocardial and cerebral infarctions (*1–3*). Evaluation of the vulnerability of atherosclerotic lesions is therefore clinically important for stratifying risk and providing early treatment. At present, however, no noninvasive diagnostic tools for the evaluation of plaque vulnerability are available for routine clinical use. Accordingly, the development of such noninvasive tools is urgently required.

Oxidized low-density lipoprotein (LDL) has been implicated in the pathogenesis of atherosclerosis and atherosclerotic plaque rupture by promoting lipid accumulation and vascular dysfunction. Lectinlike oxidized LDL receptor 1 (LOX-1) mediates the biologic effects of oxidized LDL in this process (*4*). Studies with cultured cells have suggested that LOX-1 may play several important roles in the destabilization of atherosclerotic plaques (*5–9*). Furthermore, our recent animal study indicated that LOX-1 expression in atherosclerotic plaques was positively correlated with plaque instability in vivo (*10*). Accordingly, the detection of LOX-1 expression may help assess the vulnerability of atherosclerotic plaques.

Nuclear medicine imaging enables the visualization of specific molecular processes in vivo and could be used for

Received Dec. 2, 2007; revision accepted Jun. 2, 2008.
For correspondence or reprints contact: Hideo Saji, Department of Patho-Functional Bioanalysis, Graduate School of Pharmaceutical Sciences, Kyoto University, Yoshida Shimoadachi-cho, Sakyo-ku, Kyoto 606-8501, Japan.
E-mail: hsaji@pharm.kyoto-u.ac.jp

imaging of the in vivo biologic properties of atherosclerotic plaques beyond morphologic information (*11,12*). The development of radiopharmaceuticals for the evaluation of plaque vulnerability is a matter of great concern in the clinical diagnosis of atherosclerosis.

In this study, we designed and prepared ^{99m}Tc-labeled anti–LOX-1 monoclonal IgG (^{99m}Tc-LOX-1-mAb) for investigation as an atherosclerosis imaging agent and ^{99m}Tc-labeled control mouse IgG2a (^{99m}Tc-IgG2a) for use as a control probe. Using an atherosclerosis model (myocardial infarction–prone Watanabe heritable hyperlipidemic [WHHLMI] rabbits) (*13*), we compared the accumulation of ^{99m}Tc-LOX-1-mAb and ^{99m}Tc-IgG2a in atherosclerotic lesions with histologic characteristics. Using these data, we evaluated the usefulness of ^{99m}Tc-LOX-1-mAb as an atherosclerosis imaging agent.

MATERIALS AND METHODS

Design and Preparation of ^{99m}Tc-LOX-1-mAb and ^{99m}Tc-IgG2a

A monoclonal antibody for rabbit LOX-1 (mouse IgG2a subtype) was established by use of a standard hybridoma technique (*10,14*). ^{99m}Tc-pertechnetate ($^{99m}TcO_4^-$) from Daiichi Radioisotope Laboratory generators was eluted in saline solution on a daily basis.

Anti–LOX-1 monoclonal IgG (LOX-1-mAb) was radiolabeled with ^{99m}Tc (^{99m}Tc-LOX-1-mAb) after derivatization with 6-hydrazinonicotinic acid (HYNIC) (*15*) according to a previously reported procedure (*16*) with slight modifications. In brief, HYNIC-*N*-hydroxysuccinimide was reacted with LOX-1-mAb, and the mixture was purified by size exclusion chromatography (Sephadex G-50 Fine; Amersham Pharmacia Biotech). To the purified solution of HYNIC–LOX-1-mAb was added an equal volume of ^{99m}Tc-$(tricine)_2$, prepared by the method of Larsen et al. (*17*), to obtain ^{99m}Tc-LOX-1-mAb. After purification of ^{99m}Tc-LOX-1-mAb by centrifugation of a size exclusion column with Sephadex G-50 Fine, the radiochemical purity of ^{99m}Tc-LOX-1-mAb was determined by cellulose acetate electrophoresis (Separax; Joko Co. Ltd.) to be 95.4% ± 2.2% (mean ± SD).

For the control study, negative control mouse IgG2a (Medical & Biologic Laboratories Co. Ltd.) was used for the preparation of ^{99m}Tc-IgG2a [with HYNIC and $(tricine)_2$]. The radiochemical purity of ^{99m}Tc-mouse IgG2a was 97.5% ± 0.9%.

Animal Preparation

All experimental procedures were approved by the Kyoto University Animal Care Committee. Three New Zealand White (NZW) rabbits (male, 3 mo old; Biotec, Inc.) were used to obtain peritoneal macrophages. For ^{99m}Tc-LOX-1-mAb biodistribution studies, 8 WHHLMI rabbits (5 male and 3 female, 11–24 mo old, 3.2 ± 0.5 kg; supplied by the Institute for Experimental Animals, Kobe University School of Medicine) were used. Six NZW rabbits (4 male and 2 female, 3.0 ± 0.3 mo old, 2.6 ± 0.5 kg; Biotec, Inc.) were used for the control study. For ^{99m}Tc-IgG2a biodistribution studies, 3 WHHLMI rabbits (2 male and 1 female, 11–13 mo old, 2.8 ± 0.2 kg) were used. The animals were fed standard chow (type CR-3; Clea Japan Inc.) at 120 g/d and were given water ad libitum.

Immunoreactivity of HYNIC–LOX-1-mAb

Rabbit peritoneal macrophages were obtained by the method of Ishii et al. (*18*) with minor modifications. The cells were suspended in medium A (Dulbecco's modified Eagle's medium containing 1 mM glutamine, penicillin at 100 U/mL, and streptomycin at 100 μg/mL [pH 7.4] as well as 0.2% lactalbumin hydrolysate) at a final concentration of 2.5×10^6 cells/mL. Aliquots of this cell suspension were placed in plastic petri dishes and then cultured in a humidified 5% CO_2 incubator at 37°C. After 2 h, each dish was washed twice with 10 mL of medium A to remove nonadherent cells. The monolayers were cultured for 18 h at 37°C in 20 mL of medium A, and the cells were washed twice with 10 mL of medium A and then used for experiments. More than 95% of the cells were viable, as determined by the trypan blue exclusion test, and almost all of the attached cells showed positive nonspecific esterase staining.

After the macrophages were stimulated for 6 h at 37°C in 5% CO_2 with tumor necrosis factor α at 10 ng/mL (Sigma-Aldrich, Inc.), the cells (10^6) were incubated with LOX-1-mAb (5 μg/mL, 100 μL), HYNIC–LOX-1-mAb (5 μg/mL, 100 μL), or control mouse IgG2a (5 μg/mL, 100 μL) for 30 min at 4°C. This step was followed by washing and incubation with Alexa Fluor 488 goat antimouse IgG (10 μg/mL, 100 μL; Molecular Probes, Inc.) for 30 min at 4°C. For flow cytometry analysis, cells were mixed with Iso-Flow solution (Beckman Coulter Inc.) and immediately analyzed with a FACScan instrument (Becton Dickinson Inc.). Data were analyzed with FACS software (BD CellQuest Pro; BD Biosciences Inc.). The immunoreactivity of HYNIC–LOX-1-mAb was evaluated on the basis of the median fluorescence intensity relative to that of control mouse IgG2a which, in turn, was compared with that of LOX-1-mAb. The measurements were obtained 3 times with rabbit peritoneal macrophages from 3 NZW rabbits, and the ratios were expressed as mean ± SD.

Noninvasive Imaging

After 12 h of fasting, rabbits were initially anesthetized with ketamine (7 mg/kg, intramuscularly) and xylazine (1 mg/kg, intramuscularly). The anesthetic state was maintained with additional doses of ketamine and xylazine during the experimental period. The rabbits were placed on the scanner bed in the prone position to include the abdominal aorta in the field of view. ^{99m}Tc-LOX-1-mAb (1,004 ± 110 MBq, 300 μg) or ^{99m}Tc-IgG2a (733 ± 44 MBq, 300 μg) was injected into a marginal ear vein of the rabbits (3 WHHLMI rabbits and 3 control rabbits for the ^{99m}Tc-LOX-1-mAb study and 3 WHHLMI rabbits for the ^{99m}Tc-IgG2a study). At 10 min and 24 h after injection of the radiotracer, planar images were obtained for 10 min by use of a SPECT-2000H scanner (Hitachi Medical Co.) with a low-energy, high-resolution, parallel-hole collimator having a spatial resolution of 6.7 mm at full width at half maximum. Arterial blood samples were collected from an auricular artery at 24 h. All rabbits were also used in biodistribution studies.

Biodistribution Studies

After rabbits had fasted for 12 h, ^{99m}Tc-LOX-1-mAb (122 ± 65 MBq, 300 μg) or ^{99m}Tc-IgG2a was injected into a marginal ear vein of the rabbits (8 WHHLMI rabbits and 6 control rabbits for the ^{99m}Tc-LOX-1-mAb study and 3 WHHLMI rabbits for the ^{99m}Tc-IgG study). At 24 h after the injection, all of the animals were sacrificed with an overdose of pentobarbital after blood sampling. The ascending aortic arch, the thoracic aorta, the abdominal aorta, the heart, and some femoral muscle were removed. The ascending aortic arch and thoracic and abdominal aortas were cut into 1-cm

segments. Each segment was weighed and immediately fixed in a solution containing L-(+)-lysine hydrochloride (75 mM) and 4% paraformaldehyde in phosphate buffer (37.5 mM, pH 7.4) (*19*). The radioactivity in each sample was measured with a well-type γ-counter (ARC-2000; Aloka). The results were expressed as the differential uptake ratio (DUR), which was calculated as (tissue activity/tissue weight)/(injected radiotracer activity/animal body weight), with activities given in becquerels and weights given in grams. The aorta-to-blood ratio (A/B ratio) and the aorta-to-muscle ratio (A/M ratio) were calculated from the DUR for each tissue sample.

Autoradiography (ARG) Studies

A total of 8 segments, the second and fifth segments of the ascending aortic arch and the second, fifth, and eighth segments each of the thoracic and abdominal aortas, from each animal were used for ARG studies. These segments were frozen and cut into 20-μm-thick slices with a cryomicrotome. The sections were thawed and mounted on silane-coated slides, which were then placed on a phosphorimaging plate (Fuji Imaging Plate BAS-UR; Fuji Photo Film) for 24 h together with a calibrated standard ($^{99m}TcO_4^-$ solution) to obtain ^{99m}Tc-LOX-1-mAb autoradiograms. The ARG images were analyzed by use of a computerized imaging analysis system (Bio Imaging Analyzer BAS3000 and Image Gauge Software; Fuji Photo Film). The radioactivity in each region of interest (ROI) was expressed as {radioactivity in ROI (Bq/mm^2)/[injected radioactivity (Bq)/animal body weight (g)]} × 10^2.

Histologic Analysis

The tissue sections used for ARG studies were also subjected to Azan–Mallory staining and hematoxylin–eosin (HE) staining. Therefore, ARG images were coincident with Azan–Mallory and HE images. Serial sections of the slices from the ARG studies were subjected to immunohistochemical staining (for LOX-1, macrophages, and smooth muscle cells). LOX-1 immunohistochemical staining was performed with LOX-1-mAb and an Envision+ kit (Dako) with hematoxylin counterstaining. In the same manner, immunohistochemical staining for macrophages and smooth muscle cells was performed with rabbit macrophage–specific monoclonal antibody RAM-11 (Dako) and human smooth muscle actin–specific monoclonal antibody 1A4 (Dako), respectively. Immunostaining with subclass-matched irrelevant IgG served as a negative control. Azan–Mallory staining and HE staining were performed by standard procedures. LOX-1 expression density was determined as a percentage of the positively stained region by use of a VHX digital microscope (Keyence Corp.).

To evaluate the correlation of ^{99m}Tc-LOX-1-mAb accumulation with LOX-1 expression density (Fig. 1), we divided each ARG image into 4 ROIs with vertical and horizontal lines as depicted in Figure 2B (dotted line) and then transferred the ROIs to the corresponding immunohistologic image (Fig. 2D, dotted line).

Definition of Atherosclerotic Lesions

Atherosclerotic lesions in WHHLMI rabbit aortas were divided into 4 categories by use of a classification scheme based on the recommendations of the American Heart Association (AHA) (*20,21*) and involving Azan–Mallory staining and HE staining as previously described (*22*): neointimal lesions (types I–III), atheromatous lesions (type IV), fibroatheromatous lesions (types Va and Vb), and collagen-rich lesions (type Vc) (Figs. 3 and 4).

Neointimal lesions (n = 28 for ^{99m}Tc-LOX-1-mAb study and n = 7 for ^{99m}Tc-IgG2a study) were defined as having adaptive thickening of the intima consisting of mainly smooth muscle cells and few

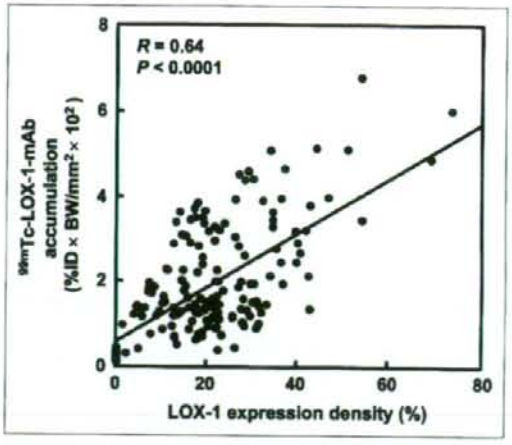

FIGURE 1. Correlation between ^{99m}Tc-LOX-1-mAb accumulation and LOX-1 expression density. Quantitative analysis of autoradiograms provided ^{99m}Tc-LOX-1-mAb accumulation, expressed as {radioactivity in ROI (Bq/mm^2)/[injected radioactivity (Bq)/animal body weight (g)]} × 10^2 (%ID × BW/mm^2 × 10^2).

macrophages. Atheromatous lesions (n = 46 and n = 20, respectively) contained thin fibrous connective tissue and a dense accumulation of extracellular lipid and foam cells and might correspond to apparently vulnerable lesions in human atherosclerotic plaques.

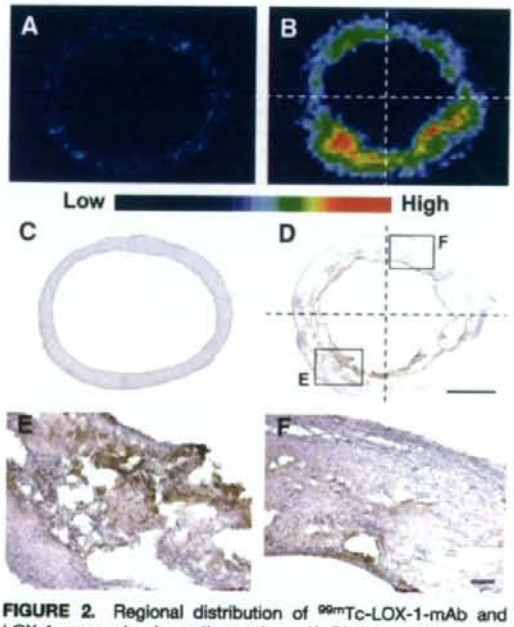

FIGURE 2. Regional distribution of ^{99m}Tc-LOX-1-mAb and LOX-1 expression in aortic sections. (A–D) Autoradiograms (A and B) and LOX-1 immunohistochemical staining (C and D) of control (A and C) and WHHLMI (B and D) rabbits. (E and F) High-magnification images of LOX-1 immunohistochemical staining from insets in D. Bars = 1 mm (C and D) and 100 μm (E and F).

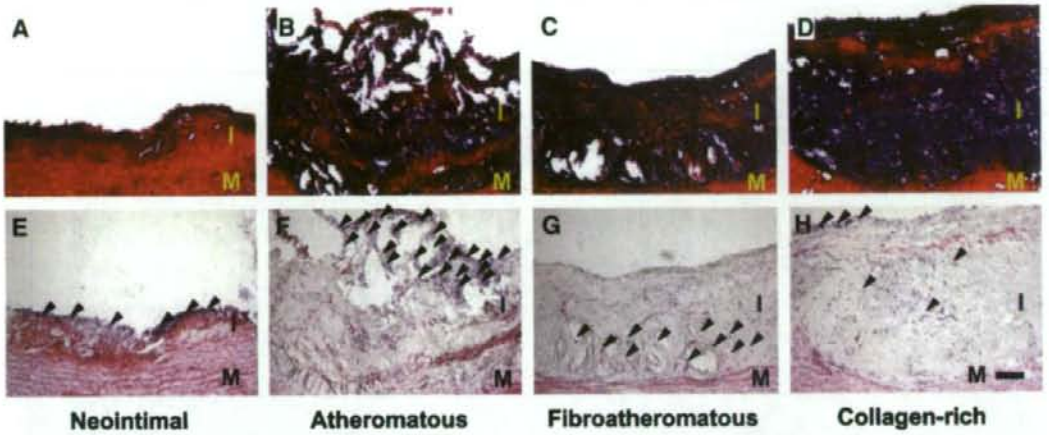

FIGURE 3. Representative photomicrographs of lesion types assigned with AHA classification scheme. (A–D) Azan–Mallory staining. (E–H) HE staining. Arrowheads mark inflammatory cell nuclei. I = intima; M = media. Bar = 100 μm.

Fibroatheromatous lesions (n = 45 and n = 17, respectively) were composed of several lipid cores separated by thick layers of fibromuscular connective tissue and might be stable against rupture (*23–25*). Collagen-rich lesions (n = 73 and n = 49, respectively) consisted of a predominantly collagenous component and contained smooth muscle cells. No lesions showed hemorrhage, plaque rupture, or thrombosis (type VI).

ROIs were placed over the atherosclerotic lesions in the WHHLMI rabbit aortic sections with reference to the classification scheme based on the Azan–Mallory and HE staining images and then were transferred to the corresponding ARG images.

Vulnerability Index

An index of morphologic destabilization characteristics, the vulnerability index, was calculated for each lesion in the WHHLMI rabbits by the method of Shiomi et al. (*26*) The vulnerability index was defined as the ratio of the lipid component area (macrophages and extracellular lipid deposits) to the fibromuscular component area (smooth muscle cells and collagen fibers). Collagen fibers and extracellular lipid deposits (extracellular vacuoles and lacunae) were determined with Azan–Mallory staining. Macrophages and smooth muscle cells were determined with immunohistochemical staining (RAM-11 and 1A4).

Statistical Analysis

Data are presented as mean ± SD. Statistical analysis was performed by use of the Mann–Whitney U test to compare aortic segments in WHHLMI and control rabbits (Table 1). Correlation coefficients were assessed by use of Spearman rank analysis (Figs. 1 and 5). Comparisons among lesion types were performed by use of the Kruskal–Wallis test, and post hoc analysis was performed by use of the Scheffe test (Fig. 6). A P value (2-tailed) of less than 0.05 was considered statistically significant.

RESULTS

Immunoreactivity of HYNIC–LOX-1-mAb

The median fluorescence intensity ratios for LOX-1-mAb and HYNIC–LOX-1-mAb relative to control mouse IgG2a were 1.63 ± 0.08 and 1.52 ± 0.11, respectively, indicating that the immunoreactivity of HYNIC–LOX-1-mAb was 93% that of LOX-1-mAb.

Noninvasive Imaging

The planar images showed primarily blood-pool radioactivity in the abdominal aorta at 10 min after the injection of ^{99m}Tc-LOX-1-mAb or ^{99m}Tc-IgG2a into WHHLMI and control rabbits (Figs. 7A–7C). At 24 h, with decreased blood-pool radioactivity in the abdominal aorta, the atherosclerotic abdominal aorta with ^{99m}Tc-LOX-1-mAb was more clearly visible than the control aorta with ^{99m}Tc-LOX-1-mAb or the atherosclerotic aorta with ^{99m}Tc-IgG2a (Figs. 7D–7F).

Biodistribution Studies

The distributions of ^{99m}Tc-LOX-1-mAb and ^{99m}Tc-IgG2a in the aortic segments of WHHLMI and control rabbits are summarized in Table 1. The level of ^{99m}Tc-LOX-1-mAb accumulation in each aortic segment in WHHLMI rabbits was 7.9- to 12.1-fold higher than that in control rabbits, and the differences were significant. A significant difference in ^{99m}Tc-LOX-1-mAb accumulation was not observed between young WHHLMI rabbits (11–13 mo) and old WHHLMI rabbits (20–24 mo) (DURs of 3.3 ± 1.4 and 2.8 ± 2.1, respectively). Blood-pool radioactivity levels (DURs) at 24 h were 4.5 ± 0.5 and 3.5 ± 0.4 in WHHLMI and control rabbits, respectively. A/B and A/M ratios were significantly higher in WHHLMI rabbits than in control rabbits. Relatively high levels of ^{99m}Tc-LOX-1-mAb accumulation were found in the liver, spleen, and kidneys in both groups of rabbits (data not shown). No marked difference in the distribution of ^{99m}Tc-LOX-1-mAb in nontarget organs was observed between WHHLMI and control rabbits.

The level of ^{99m}Tc-LOX-1-mAb accumulation in WHHLMI rabbit aortas was 1.8- to 2.5-fold higher than the level of ^{99m}Tc-IgG2a accumulation, and the differences were significant.

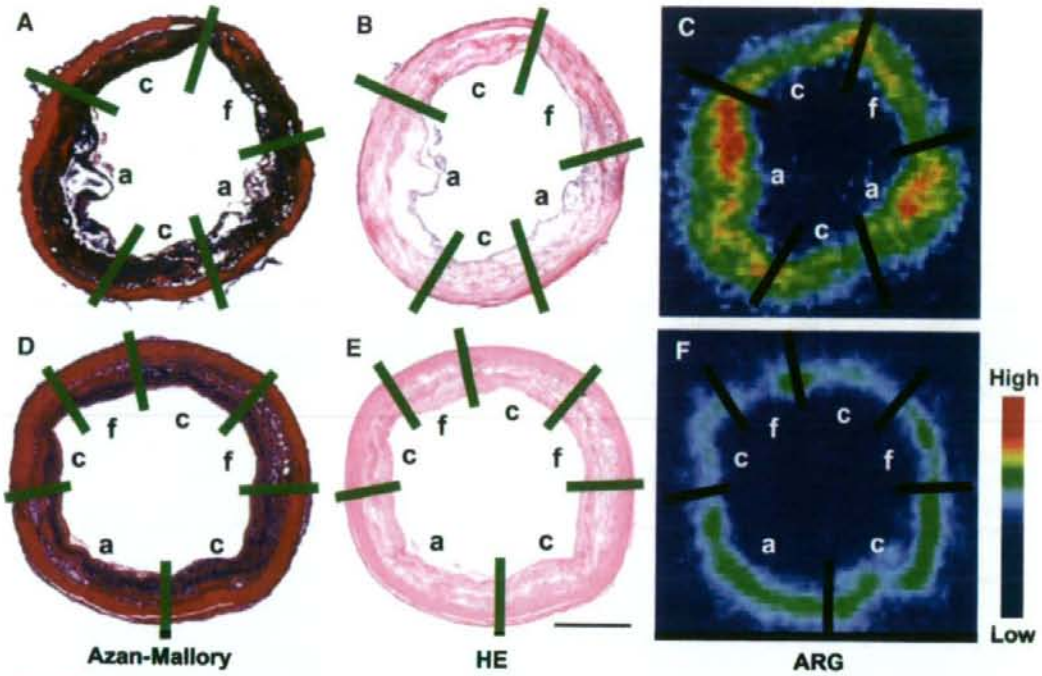

FIGURE 4. Lesion classification scheme in representative photomicrographs and autoradiograms of cross sections of WHHLMI rabbit aortas in ^{99m}Tc-LOX-1-mAb study (A–C) and ^{99m}Tc-IgG2a study (D–F). Atherosclerotic lesions were assigned with AHA classification scheme from Azan–Mallory staining (A and D) and HE staining (B and E) (Fig. 3). Same classification was applied to autoradiograms (ARG) (C and F). ROIs were placed over atherosclerotic lesions in WHHLMI rabbit aortic sections by reference to images with classification scheme from Azan–Mallory staining. a = atheromatous lesions; c = collagen-rich lesions; f = fibroatheromatous lesions. Bar = 1 mm.

Correlation of Regional Distribution of ^{99m}Tc-LOX-1-mAb with LOX-1 Expression

In the ARG studies, heterogeneous ^{99m}Tc-LOX-1-mAb accumulation was observed in the intima of the WHHLMI rabbit aortas, whereas there was little accumulation in the aortas of control rabbits (Figs. 2A and 2B). LOX-1 expression was detected in intimal lesions in WHHLMI rabbit aortas, and the levels of expression differed among the regions (Fig. 2D). As shown in Figures 2B and 2D, higher levels of accumulation of ^{99m}Tc-LOX-1-mAb were observed in regions with high levels of LOX-1 expression, whereas lower levels of accumulation were seen in regions with low levels of LOX-1 expression. Consequently, regional ^{99m}Tc-LOX-1-mAb accumulation in WHHLMI rabbit aortic sections was significantly correlated with LOX-1 expression density ($r = 0.64$, $P < 0.0001$) (Fig. 1). No obvious LOX-1 expression was observed in the aortas of control rabbits (Fig. 2C).

Correlation of Accumulation of ^{99m}Tc-LOX-1-mAb and ^{99m}Tc-IgG2a with Histologic Characteristics

^{99m}Tc-LOX-1-mAb accumulation was dependent on the histologic grade of lesions (Figs. 4C and 6A), and the highest (and significant; $P < 0.0001$) level was seen in atheromatous lesions (type IV), followed in decreasing order by fibroatheromatous, collagen-rich, and neointimal lesions. Figures 6B and 6C show the macrophage density and vulnerability index quantified for each lesion in the ^{99m}Tc-LOX-1-mAb study. The macrophage density and vulnerability index were also the highest in atheromatous lesions, followed in decreasing order by fibroatheromatous, neointimal, and collagen-rich lesions. Consequently, the highest values for ^{99m}Tc-LOX-1-mAb accumulation, macrophage density, and the vulnerability index were observed in atheromatous lesions. In contrast, lower values for ^{99m}Tc-LOX-1-mAb accumulation, macrophage density, and the vulnerability index were seen in collagen-rich and neointimal lesions. Figure 5A shows the regression analysis for ^{99m}Tc-LOX-1-mAb accumulation and the vulnerability index. The regression analysis demonstrated a directly proportional relationship between ^{99m}Tc-LOX-1-mAb accumulation and the vulnerability index ($r = 0.67$, $P < 0.0001$).

In contrast, control tracer (^{99m}Tc-IgG2a) accumulation was independent of the histologic grade of lesions, and the differences among the lesions were not significant (Figs. 4F

TABLE 1
Distributions of ^{99m}Tc-LOX-1-mAb and ^{99m}Tc-IgG2a in Aortic Segments of Control and WHHLMI Rabbits at 24 Hours After Injection

Parameter	Mean ± SD for: ^{99m}Tc-LOX-1-mAb in: Control rabbits	^{99m}Tc-LOX-1-mAb in: WHHLMI rabbits	^{99m}Tc-IgG2a in WHHLMI rabbits
Aortic segment*			
Arch (ascending)	0.45 ± 0.19†	4.0 ± 2.0‡	1.6 ± 0.4†
Thoracic	0.29 ± 0.17†	3.5 ± 1.1‡	1.9 ± 0.3†§
Abdominal	0.29 ± 0.15†	2.3 ± 1.2	1.3 ± 0.6‖
Total	0.32 ± 0.17†	3.2 ± 1.6	1.6 ± 0.5†
A/B ratio	0.12 ± 0.08†	0.69 ± 0.33	0.33 ± 0.11†
A/M ratio	3.1 ± 1.4‡	30.8 ± 16.5	18.1 ± 9.8†

*Reported as DUR.
†$P < 0.0001$ vs. WHHLMI rabbits in ^{99m}Tc-LOX-1-mAb study.
‡$P < 0.0001$ vs. abdominal aorta.
§$P < 0.001$ vs. abdominal aorta.
‖$P < 0.05$ vs. WHHLMI rabbits in ^{99m}Tc-LOX-1-mAb study.
Accumulation in each aortic segment was significantly higher in WHHLMI rabbits than in control rabbits. Ascending arch of aorta and thoracic aorta showed higher radioactivity than abdominal aorta in WHHLMI rabbits.

and 6C). The ^{99m}Tc-IgG2a distribution based on the lesion classification was different from that of ^{99m}Tc-LOX-1-mAb, although the distributions of macrophage density and the vulnerability index in the ^{99m}Tc-IgG2a study were similar to those in the ^{99m}Tc-LOX-1-mAb study (data not shown). Furthermore, no correlation between ^{99m}Tc-IgG2a accumulation and the vulnerability index was shown ($r = 0.002$, $P < 0.0001$) (Fig. 5B).

DISCUSSION

There is an urgent need to develop a means to discriminate vulnerable atherosclerotic lesions (atheromatous lesions) from potentially stable lesions in clinical practice, because the disruption of vulnerable plaques causes myocardial and cerebral infarctions. In the present study, we designed and prepared a new imaging agent, ^{99m}Tc-LOX-1-mAb. Our results clearly indicated the potential of ^{99m}Tc-LOX-1-mAb for targeting LOX-1 and evaluating the vulnerability of atherosclerotic lesions.

The immunoreactivity of an agent is an essential factor in in vivo imaging with immunodetection. Flow cytometry analyses indicated that the modification of LOX-1-mAb with the chelating moiety (HYNIC) did not significantly affect the immunoreactivity of the original LOX-1-mAb, although the mean fluorescence intensity was low. Furthermore, ARG and immunohistochemical studies showed that ^{99m}Tc-LOX-1-mAb accumulation in atherosclerotic lesions was well correlated with LOX-1 expression density (Fig. 1). These results suggested the potential of ^{99m}Tc-LOX-1-mAb to specifically recognize LOX-1 in vivo.

The highest level of ^{99m}Tc-LOX-1-mAb accumulation was seen in atheromatous lesions (Fig. 6A) and was significantly correlated with the vulnerability index (Fig. 5A), indicating the ability of this agent to distinguish apparently vulnerable atheromatous lesions from more stable, chronic plaques. This result is consistent with the in vivo relationship between LOX-1 expression and lesion vulnerability (*10*). In contrast, the relationship between ^{99m}Tc-LOX-1-mAb accu-

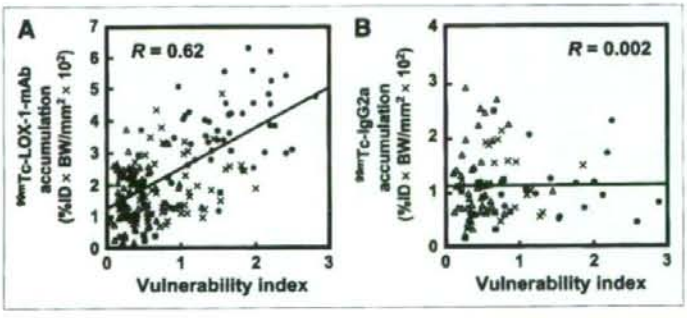

FIGURE 5. Simple regression analyses of vulnerability index with ^{99m}Tc-LOX-1-mAb accumulation (A) and ^{99m}Tc-IgG2a accumulation (B). See legend to Fig. 1 for explanation of units. ● = atheromatous lesion; △ = collagen-rich lesion; × = fibroatheromatous lesion; ■ = neointimal lesion.

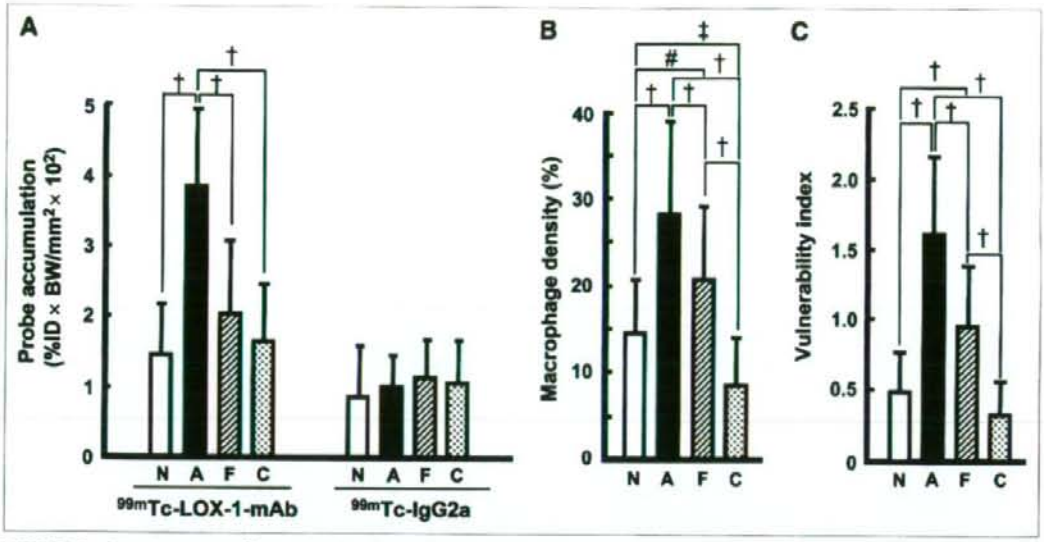

FIGURE 6. Distributions of ^{99m}Tc-LOX-1-mAb and ^{99m}Tc-IgG2a (A) and macrophage density (B) and vulnerability index (C) for each lesion type in ^{99m}Tc-LOX-1-mAb study. Quantitative analysis of autoradiograms provided ^{99m}Tc-LOX-1-mAb and ^{99m}Tc-IgG2a accumulation, expressed as %ID × BW/mm² × 10² (see legend to Fig. 1 for explanation of units). Data are presented as mean ± SD. †$P < 0.0001$. ‡$P < 0.01$. #$P < 0.05$. A = atheromatous lesions; C = collagen-rich lesions; F = fibroatheromatous lesions; N = neointimal lesions.

mulation (LOX-1 signal) and macrophage density was not high ($r = 0.49$, $P < 0.001$) (data not shown), compared with the relationship with the vulnerability index (Fig. 5A). It has been reported that LOX-1 is intensely expressed in endothelial cells and macrophages (foam cells) in unstable atherosclerotic plaques (*10,27*). In the present study, LOX-1 expression was mainly observed in macrophages; however, LOX-1 was also expressed in endothelial cells and smooth muscle cells. LOX-1 plays multiphasic roles in the formation of vulnerable atherosclerotic plaques (*5–9*). Accordingly, although ^{99m}Tc-LOX-1-mAb accumulation is not highly correlated with macrophage density, ^{99m}Tc-LOX-1-mAb should provide clinically useful information about atherogenesis on the basis of the LOX-1 expression level.

In the present study, we applied a nuclear imaging technique for atherosclerosis imaging. Nuclear imaging is used with the aim of visualizing the biologic properties of atherosclerotic plaques (e.g., cellular composition, inflammatory

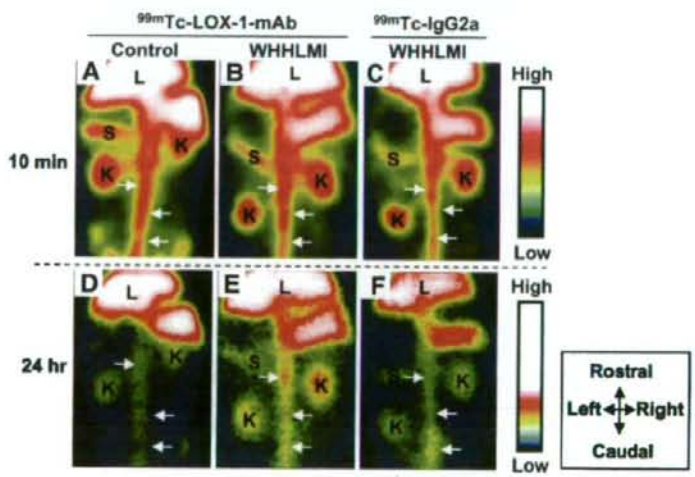

FIGURE 7. Noninvasive imaging of abdominal region with ^{99m}Tc-LOX-1-mAb (A, B, D, and E) and ^{99m}Tc-IgG2a (C and F). Planar images for WHHLMI (B, C, E, and F) and control (A and D) rabbits at 10 min (A–C) and 24 h (D–F) after injection are shown. Field of view = 170 × 120 mm. Arrows = aorta; K = kidney; L = liver; S = spleen.

cell activity, receptor expression, or apoptotic events) (*11,12*). Accordingly, nuclear imaging approaches could provide new diagnostic imaging capabilities for detecting vulnerable plaques on the basis of a specific biologic aspect of atherosclerosis progression. Tsimikas et al. reported the use of a ^{99m}Tc-oxidized LDL–specific antibody for atherosclerosis imaging (*28,29*); this agent allowed the detection of atherosclerosis progression and regression. However, oxidized LDL would need to be injected after the use of this agent to reduce a high level of accumulation of the antibody in the blood and liver. Furthermore, LOX-1 may be a more suitable target than oxidized LDL because it is a specific factor in atherosclerosis progression and is expressed during the early period of atherosclerosis. In contrast, nonspecific uptake into atherosclerosis lesions and high permeability of lesions are important concerns (*30,31*). Therefore, we performed a ^{99m}Tc-IgG2a (control probe) study, which showed the specific uptake of ^{99m}Tc-LOX-1-mAb in atherosclerotic plaques.

As representative nuclear imaging probes, ^{18}F-FDG for imaging metabolic activity in macrophages (*19,32*) and ^{99m}Tc-annexin A5 for imaging apoptosis (*33,34*) were recently used for atherosclerotic plaque imaging. Consequently, it was especially important and intriguing to characterize ^{99m}Tc-LOX-1-mAb in the same animal model (WHHLMI rabbits), focusing on the advantages of ^{99m}Tc-LOX-1-mAb. First, the levels of ^{99m}Tc-LOX-1-mAb accumulation were 2.4- and 3.2-fold higher than the levels of ^{18}F-FDG accumulation (DURs, 1.47 ± 0.90 and 0.72 ± 0.37) in the thoracic and abdominal aortic segments in WHHLMI rabbits, respectively (*19*). Additionally, the level of ^{99m}Tc-LOX-1-mAb accumulation was 5.2-fold higher than the level of ^{99m}Tc-annexin A5 accumulation (DUR, 0.64 ± 0.18 [total aorta]) in aortic segments in WHHLMI rabbits (*33*). These results indicated the potential of ^{99m}Tc-LOX-1-mAb for in vivo imaging, as the accumulation level is an essential factor for this purpose.

Second, ^{99m}Tc-LOX-1-mAb accumulated predominantly in atheromatous lesions. The accumulation ratios of ^{99m}Tc-LOX-1-mAb for atheromatous lesions to other lesions (atheromatous/neointimal, atheromatous/fibroatheromatous, and atheromatous/collagen-rich lesion ratios) were higher than those of ^{99m}Tc-annexin A5 (2.7 vs. 1.3, 1.9 vs. 1.3, and 2.4 vs. 1.8, respectively), indicating that ^{99m}Tc-LOX-1-mAb accumulated more selectively in atheromatous lesions. These results suggested the ability of ^{99m}Tc-LOX-1-mAb to selectively detect vulnerable plaques among heterogeneous atherosclerotic lesions.

In noninvasive imaging studies with ^{99m}Tc-LOX-1-mAb, the atherosclerotic abdominal aorta was imaged more clearly in WHHLMI rabbits than in control rabbits, with decreased blood-pool radioactivity in the abdominal aorta (Fig. 7). This result was confirmed in biodistribution studies (Table 1). However, the difference between control and WHHLMI rabbits seemed to be underwhelming when determined from ARG images, for various reasons. First, the spatial resolution of the SPECT images (6.7 mm at full width at half maximum) was lower than that of the ARG images (50 μm). Second, the A/B ratio in WHHLMI rabbits was 0.69 ± 0.33 at 24 h, indicating that the radioactivity detected by noninvasive imaging was attributable to both aorta and blood radioactivity, although this A/B ratio was comparable to that of ^{99m}Tc-annexin A5 (1.0 ± 0.2 at 3 h after injection). Johnson et al. reported the possibility of in vivo imaging of porcine coronary lesions with ^{99m}Tc-annexin A5 (*35*). However, further studies on the acceleration of clearance of radioactivity from the blood pool are necessary. It has been reported that radiopharmaceuticals derived from low-molecular-weight polypeptides or compounds, small recombinant antibody fragments (Fab and scFv), engineered variants (diabodies, triabodies, minibodies, and single-domain antibodies), and pretargeting antibody methods show rapid clearance of radioactivity from the circulation (*36–38*). The technical progression of SPECT devices could also eliminate the high-background problem.

CONCLUSION

We designed and prepared ^{99m}Tc-LOX-1-mAb for the imaging of LOX-1 and characterized the accumulation of ^{99m}Tc-LOX-1-mAb in atherosclerotic lesions in a rabbit model of spontaneous atherosclerosis. We demonstrated that ^{99m}Tc-LOX-1-mAb could evaluate lesion vulnerability more sensitively than other imaging probes. It could be applied in the clinical setting because of the similarity of the histologic characteristics of atherosclerotic plaques in humans and WHHLMI rabbits. ^{99m}Tc-LOX-1-mAb could be useful as a potential imaging probe for predicting lesions prone to spontaneous rupture and monitoring the effects of timely treatment in patients with advanced atherosclerosis.

ACKNOWLEDGMENTS

This work was partly supported by a Grant-in-Aid for General Scientific Research from the Ministry of Education, Culture, Sports, Science and Technology of Japan and from the Japan Society for the Promotion of Science, by a research grant from the New Energy and Industrial Technology Development Organization (NEDO), by a research grant for cardiovascular diseases from the Ministry of Health, Labor and Welfare (16C-8), and by the 21st Century COE Program "Knowledge Information Infrastructure for Genome Science."

REFERENCES

1. Lendon C, Born GV, Davies MJ, Richardson PD. Plaque fissure: the link between atherosclerosis and thrombosis. *Nouv Rev Fr Hematol.* 1992;34:27–29.
2. Ruberg FL, Leopold JA, Loscalzo J. Atherothrombosis: plaque instability and thrombogenesis. *Prog Cardiovasc Dis.* 2002;44:381–394.
3. Kolodgie FD, Virmani R, Burke AP, et al. Pathologic assessment of the vulnerable human coronary plaque. *Heart.* 2004;90:1385–1391.
4. Sawamura T, Kume N, Aoyama T, et al. An endothelial receptor for oxidized low-density lipoprotein. *Nature.* 1997;386:73–77.

5. Kume N, Kita T. Roles of lectin-like oxidized LDL receptor-1 and its soluble forms in atherogenesis. *Curr Opin Lipidol.* 2001;12:419–423.
6. Moriwaki H, Kume N, Kataoka H, et al. Expression of lectin-like oxidized low density lipoprotein receptor-1 in human and murine macrophages: upregulated expression by TNF-alpha. *FEBS Lett.* 1998;440:29–32.
7. Kataoka H, Kume N, Miyamoto S, et al. Oxidized LDL modulates Bax/Bcl-2 through the lectinlike Ox-LDL receptor-1 in vascular smooth muscle cells. *Arterioscler Thromb Vasc Biol.* 2001;21:955–960.
8. Kume N, Kita T. Apoptosis of vascular cells by oxidized LDL: involvement of caspases and LOX-1 and its implication in atherosclerotic plaque rupture. *Circ Res.* 2004;94:269–270.
9. Li D, Liu L, Chen H, et al. LOX-1 mediates oxidized low-density lipoprotein-induced expression of matrix metalloproteinases in human coronary artery endothelial cells. *Circulation.* 2003;107:612–617.
10. Ishino S, Mukai T, Kume N, et al. Lectin-like oxidized LDL receptor-1 (LOX-1) expression is associated with atherosclerotic plaque instability: analysis in hypercholesterolemic rabbits. *Atherosclerosis.* 2007;195:48–56.
11. Jaffer FA, Libby P, Weissleder R. Molecular and cellular imaging of atherosclerosis: emerging applications. *J Am Coll Cardiol.* 2006;47:1328–1338.
12. Davies JR, Rudd JH, Weissberg PL. Molecular and metabolic imaging of atherosclerosis. *J Nucl Med.* 2004;45:1898–1907.
13. Shiomi M, Ito T, Yamada S, et al. Development of an animal model for spontaneous myocardial infarction (WHHLMI rabbit). *Arterioscler Thromb Vasc Biol.* 2003;23:1239–1244.
14. Eto H, Miyata M, Kume N, et al. Expression of lectin-like oxidized LDL receptor-1 in smooth muscle cells after vascular injury. *Biochem Biophys Res Commun.* 2006;341:591–598.
15. Abrams MJ, Juweid M, tenKate CI, et al. Technetium-99m-human polyclonal IgG radiolabeled via the hydrazino nicotinamide derivative for imaging focal sites of infection in rats. *J Nucl Med.* 1990;31:2022–2028.
16. Ono M, Arano Y, Mukai T, et al. Plasma protein binding of ^{99m}Tc-labeled hydrazino nicotinamide derivatized polypeptides and peptides. *Nucl Med Biol.* 2001;28:155–164.
17. Larsen SK, Solomon HF, Caldwell G, et al. [^{99m}Tc]tricine: a useful precursor complex for the radiolabeling of hydrazinonicotinate protein conjugates. *Bioconjug Chem.* 1995;6:635–638.
18. Ishii K, Kita T, Kume N, Nagano Y, Kawai C. Uptake of acetylated LDL by peritoneal macrophages obtained from normal and Watanabe heritable hyperlipidemic rabbits, an animal model for familial hypercholesterolemia. *Biochim Biophys Acta.* 1988;962:387–389.
19. Ogawa M, Ishino S, Mukai T, et al. ^{18}F-FDG accumulation in atherosclerotic plaques: immunohistochemical and PET imaging study. *J Nucl Med.* 2004;45:1245–1250.
20. Stary HC, Chandler AB, Glagov S, et al. A definition of initial, fatty streak, and intermediate lesions of atherosclerosis: a report from the Committee on Vascular Lesions of the Council on Arteriosclerosis, American Heart Association. *Circulation.* 1994;89:2462–2478.
21. Stary HC, Chandler AB, Dinsmore RE, et al. A definition of advanced types of atherosclerotic lesions and a histological classification of atherosclerosis: a report from the Committee on Vascular Lesions of the Council on Arteriosclerosis, American Heart Association. *Circulation.* 1995;92:1355–1374.
22. Kobayashi S, Inoue N, Ohashi Y, et al. Interaction of oxidative stress and inflammatory response in coronary plaque instability: important role of C-reactive protein. *Arterioscler Thromb Vasc Biol.* 2003;23:1398–1404.
23. Shiomi M, Ito T, Hirouchi Y, et al. Stability of atheromatous plaque affected by lesional composition: study of WHHL rabbits treated with statins. *Ann N Y Acad Sci.* 2001;947:419–423.
24. Mann JM, Davies MJ. Vulnerable plaque: relation of characteristics to degree of stenosis in human coronary arteries. *Circulation.* 1996;94:928–931.
25. Falk E, Shah PK, Fuster V. Coronary plaque disruption. *Circulation.* 1995;92:657–671.
26. Shiomi M, Ito T, Hirouchi Y, et al. Fibromuscular cap composition is important for the stability of established atherosclerotic plaques in mature WHHL rabbits treated with statins. *Atherosclerosis.* 2001;157:75–84.
27. Chen M, Kakutani M, Minami M, et al. Increased expression of lectin-like oxidized low density lipoprotein receptor-1 in initial atherosclerotic lesions of Watanabe heritable hyperlipidemic rabbits. *Arterioscler Thromb Vasc Biol.* 2000;20:1107–1115.
28. Tsimikas S, Palinski W, Halpern SE, Yeung DW, Curtiss LK, Witztum JL. Radiolabeled MDA2, an oxidation-specific, monoclonal antibody, identifies native atherosclerotic lesions in vivo. *J Nucl Cardiol.* 1999;6:41–53.
29. Tsimikas S, Shaw PX. Non-invasive imaging of vulnerable plaques by molecular targeting of oxidized LDL with tagged oxidation-specific antibodies. *J Cell Biochem Suppl.* 2002;39:138–146.
30. Christensen S, Nielsen H. Permeability of arterial endothelium to plasma macromolecules. *Atherosclerosis.* 1977;27:447–463.
31. Smith EB, Staples EM. Distribution of plasma proteins across the human aortic wall: barrier functions of endothelium and internal elastic lamina. *Atherosclerosis.* 1980;37:579–590.
32. Rudd JH, Warburton EA, Fryer TD, et al. Imaging atherosclerotic plaque inflammation with [^{18}F]-fluorodeoxyglucose positron emission tomography. *Circulation.* 2002;105:2708–2711.
33. Ishino S, Kuge Y, Takai N, et al. ^{99m}Tc-annexin A5 for noninvasive characterization of atherosclerotic lesions: imaging and histological studies in myocardial infarction-prone Watanabe heritable hyperlipidemic rabbits. *Eur J Nucl Med Mol Imaging.* 2007;34:889–899.
34. Kietselaer BL, Reutelingsperger CP, Heidendal GA, et al. Noninvasive detection of plaque instability with use of radiolabeled annexin A5 in patients with carotid-artery atherosclerosis. *N Engl J Med.* 2004;350:1472–1473.
35. Johnson LL, Schofield L, Donahay T, et al. ^{99m}Tc-annexin V imaging for in vivo detection of atherosclerotic lesions in porcine coronary arteries. *J Nucl Med.* 2005;46:1186–1193.
36. Behr TM, Becker WS, Bair HJ, et al. Comparison of complete versus fragmented technetium-99m-labeled anti-CEA monoclonal antibodies for immunoscintigraphy in colorectal cancer. *J Nucl Med.* 1995;36:430–441.
37. Sharkey RM, Karacay H, Cardillo TM, et al. Improving the delivery of radionuclides for imaging and therapy of cancer using pretargeting methods. *Clin Cancer Res.* 2005;11:7109–7121.
38. Sakahara H, Saga T. Avidin-biotin system for delivery of diagnostic agents. *Adv Drug Deliv Rev.* 1999;37:89–101.

Distribution Profiles of Membrane Type-1 Matrix Metalloproteinase (MT1-MMP), Matrix Metalloproteinase-2 (MMP-2) and Cyclooxygenase-2 (COX-2) in Rabbit Atherosclerosis: Comparison with Plaque Instability Analysis

Yuji KUGE,*[,a] Nozomi TAKAI,[a] Seigo ISHINO,[a] Takashi TEMMA,[a] Masashi SHIOMI,[b] and Hideo SAJI[a]

[a] *Department of Patho-functional Bioanalysis, Graduate School of Pharmaceutical Sciences, Kyoto University; 46–29 Yoshida Shimoadachi-cho, Sakyo-ku, Kyoto 606–8501, Japan: and* [b] *Institute for Experimental Animals, Kobe University School of Medicine; 7–5–1 Kusunokicho, Chuo-ku, Kobe 650–0017, Japan.*
Received March 3, 2007; accepted June 27, 2007; published online July 6, 2007

Background: Despite increasing evidence that membrane type 1 matrix metalloproteinase (MT1-MMP), matrix metalloproteinase-2 (MMP-2), and cyclooxygenase-2 (COX-2) are involved in the pathogenesis of atherosclerosis, the possible links among these enzymes remain unclear. Accordingly, we investigated the distribution of MT1-MMP, MMP-2, and COX-2 immunohistologically in the atherosclerotic lesions of hypercholesterolemic (WHHLMI) rabbits. Methods and Results: Distribution of MT1-MMP, MMP-2, and COX-2 was examined by immunohistochemical staining using sixty cross sections of the ascending-arch and thoracic aortas prepared from 4 WHHLMI rabbits. MT1-MMP and MMP-2 staining was prominently observed in the macrophage-rich regions of the atheromatous lesions, and was positively correlated with morphological vulnerability ($r=0.63$ for MT1-MMP; $r=0.60$ for MMP-2; $p<0.0001$). MT1-MMP staining was positively correlated with MMP-2 staining ($r=0.61$, $p<0.0001$). COX-2 staining was also the highest in the macrophage-rich regions of the atheromatous lesions, with relatively high staining levels in other more stable lesions. Conclusions: Co-distribution of MT1-MMP, MMP-2, and COX-2 was demonstrated in grade IV atheroma, indicating a possible link among these enzymes in the destabilization of atherosclerotic plaques. The relatively high COX-2 distribution in other more stable lesions may indicate its additional roles in the stabilization of atherosclerotic lesions. The present findings in hypercholesterolemic rabbits should help advance our understanding of the pathophysiology of atherosclerosis and provide useful information for the development of new therapeutic and diagnostic (imaging) agents that target MMPs and COX-2 in atherosclerosis.

Key words atherosclerosis; matrix metalloproteinase; cyclooxygenase; rabbit; plaque

Our current understanding of the pathophysiology of atherosclerosis suggests the involvement of complex mechanisms that go beyond mere lipid storage disorders.[1,2] It is of great importance to investigate causative factors in the destabilization of atherosclerotic plaques, which should help develop new therapeutic and diagnostic (imaging) agents of atherosclerosis, leading to the establishment of novel therapeutic strategies for preventing acute coronary syndromes and stroke.

To date, several factors, including enhanced inflammatory responses and expression of matrix metalloproteinases (MMPs), have been suggested to play important roles in the destabilization of atherosclerotic plaques.[1—4] Plaques prone to rupture are morphologically characterized by a thin fibrous cap overlying a large lipid core. MMPs have been shown to degrade extracellular matrix (ECM) that constitutes the fibrous cap of the plaques, resulting in the destabilization of atherosclerotic plaques.[3—5] Increased expression of MMP-2 and MMP-9 has been demonstrated within human atherosclerotic lesions and critically implicated in plaque rupture.[5—7] MMP-2 and MMP-9 are known to cleave native type IV, V, VII, and X collagens and elastin, as well as the products of collagens types I, II, and III after proteolysis by collagenases, such as MMP-1 and MMP-13, and are considered to be involved in plaque instability.[3] The MMPs can be divided into two groups: soluble MMPs and membrane-bound MMPs. Most soluble MMPs, including MMP-2 and MMP-9, are released from cells as zymogens and require extracellular posttranslational cleavage to gain biological activity.[3,8] A membrane-bound MMP, membrane type-1 MMP (MT1-MMP or MMP-14), has been demonstrated to mediate the activation of pro-MMP-2 to active MMP-2 on the cell surface.[8,9] The expression of MT1-MMP has also been found within human atherosclerotic plaques.[10,11] Thus, MT1-MMP, an activator of pro-MMP-2 to active MMP-2, has been speculated to be an important determinant of the destabilization of atherosclerotic plaques.

Production of MMP-2 and MMP-9 by monocytes/macrophages occurs through a prostaglandin (PG) E_2/cAMP-dependent pathway.[1,12,13] Recently, Shankavaram *et al.* demonstrated that induction of monocyte MT1-MMP is also regulated through the PG E_2/cAMP pathway.[14] These findings indicate the involvement of cyclooxygenases (COXs), rate-limiting enzymes in the conversion of arachidonic acid into PGs and thromboxanes, in the regulation of MMP biosynthesis.[1,15] To date, at least 2 distinct isoforms of the COXs—a constitutive form (COX-1) and an inducible isoform (COX-2)—and several of their variants have been discovered.[16] COX-1 is constitutively expressed in most tissues and is responsible for maintaining homeostasis, whereas COX-2 is induced in response to inflammatory stimuli.[17] Overexpression of COX-2 has been shown within human atherosclerotic plaques, localized predominantly in macrophages/foam cells, and to a lesser extent in medial smooth muscle cells and endothelial cells.[18,19] Extensive studies by Cipollone *et al.* have provided evidence that COX-2 expression is associated with acute ischemic syndromes, possibly through MMP-2/MMP-9 induced plaque

* To whom correspondence should be addressed. e-mail: kuge@pharm.kyoto-u.ac.jp

rupture.[3,12,20] Hong *et al.* reported the coexpression of COX-2 and MT1-MMP in the atherosclerotic intima, plaque itself, and vascular smooth muscle cells in patients with atherosclerotic aortic aneurysm and dissection.[21]

Taken together, the signaling cascade, namely, activation of pro-MMP-2 to active MMP-2 by MT1-MMP through the PG E_2/cAMP pathway, may play pivotal roles in the destabilization of atherosclerotic plaques. However, the roles of the possible links among MT1-MMP, MMP-2, and COX-2 in the pathophysiology of atherosclerosis have not been fully investigated. To the best of our knowledge, there has been no report that directly compared the distribution profiles of MT1-MMP, MMP-2, and COX-2 in atherosclerotic lesions *in vivo*.

Watanabe heritable hyperlipidemic (WHHL) rabbits and a current strain of the rabbits, myocardial infarction-prone Watanabe heritable hyperlipidemic (WHHLMI) rabbits, have been widely used as animal models of spontaneous atherosclerosis because the pathological characteristics have been reported to be relevant to human atherosclerosis.[22,23] The use of WHHLMI rabbits could be effective for investigating causative factors in the destabilization of atherosclerotic plaques, and should provide a useful means for investigating new therapeutic and diagnostic (imaging) agents of atherosclerosis. Thus, in the present study, we investigated the distribution of MT1-MMP, MMP-2, and COX-2 immunohistologically in the atherosclerotic lesions of WHHLMI rabbits, in comparison with atherosclerotic plaque instability analysis.

MATERIALS AND METHODS

Animals Four female WHHLMI rabbits (12.6±0.8 months old: 3.7±0.3 kg body weight) bred at Kobe University were used in the present study. Four Japanese White rabbits (3.1±0.1 months old: 2.7±0.1 kg body weight) purchased from Biotec. Inc. (Saga, Japan) were also used as controls. The rabbits were fed standard rabbit chow (type CR-3; Clea Japan Inc., Tokyo, Japan: 120 g/d) and were given water *ad libitum*. All experimental procedures were approved by the Kyoto University Animal Care Committee.

Preparation of Histological Sections The rabbits were sacrificed with an overdose of sodium pentobarbital. The ascending-arch and thoracic aorta were cut into 6 and 9 segments, respectively. Each segment was immediately fixed in a solution containing L-(+)-lysine hydrochloride (75 mmol/l) and 4% paraformaldehyde in phosphate buffer (37.5 mmol/l; pH 7.4), and embedded in paraffin. Consecutive 5-μm-thick slices were prepared at the center of each segment.

Histological Analysis Serial sections were subjected to immunohistochemical staining for MT1-MMP, MMP-2, COX-2 and cell type marker antigens, as well as Azan-Mallory and hematoxylin–eosin (HE) staining. Immunohistochemical staining was performed according to standard immunostaining procedures with slight modifications.[21,24–26] MT1-MMP and MMP-2 were immunostained with a purified mouse monoclonal antibody to an oligopeptide (residue 319 to 333, numbered from signal peptide) on human MT1-MMP (1 : 50 dilution; 113-5B7, mouse IgG, Daiichi Fine Chemical Co., Ltd., Toyama, Japan) and with that to an oligopeptide (residue 468 to 483, numbered from propeptide) on human MMP-2 (1 : 20 dilution; 42-5D11, mouse IgG, Daiichi Fine Chemical Co., Ltd.), respectively. These antibodies specifically recognize both pro- and active forms of the enzymes. Immunostainings for a rabbit macrophage-specific antigen (1 : 50 dilution; RAM-11, mouse IgG) and smooth muscle actin (1 : 50 dilution; 1A4, mouse IgG) were also performed using monoclonal antibodies obtained from Dako Corp., Santa Barbara, CA, U.S.A. The bound antibodies were visualized by using a DAKO Envision+ kit (Dako) and 3,3'-diaminobenzidine tetrahydrochloride (DAB) (Dako). Counterstaining with hematoxylin was performed. Immunostaining with subclass-matched irrelevant IgG served as negative controls.

For COX-2 immunostaining, deparaffinized sections were heated with a microwave oven for antigen retrieval. Thereafter, the specimens were incubated with a goat polyclonal antibody (1 : 200 dilution; sc-1745, Santa Cruz Biotechnology, Inc., CA, U.S.A.) that raised against a peptide sequence at the C-terminus of human COX-2. The bound antibody was visualized using a Dako LSAB+ kit (Dako) with hematoxylin counterstaining.

Classification of Atherosclerotic Lesions The atherosclerotic lesions in WHHLMI rabbits were divided into 4 categories using a classification scheme based on the recommendations of the American Heart Association (AHA)[27,28] by Azan-Mallory and HE staining, as previously described (13): (1) neointimal lesion (Type I—III), (2) atheromatous lesion (Type IV), (3) fibroatheromatous lesion (Type Va, Vb), (4) collagen-rich lesion (Type Vc), as shown in Fig. 2. Neointimal lesions were defined as having adaptive thickening of the intima consisting mainly of smooth muscle cells (SMCs) and few macrophages. Atheromatous lesions contained thin fibrous connective tissue and a dense accumulation of extracellular lipid and foam cells, and were considered to be vulnerable-like lesions in human atherosclerotic plaques. Fibroatheromatous lesions were composed of several lipid cores and separated by thick layers of fibromuscular connective tissue, which was relatively stable to rupture.[29] Collagen-rich lesions consisted of a predominantly collagenous component and contained smooth muscle cells. The distinction between the fibroatheromatous and collagen-rich lesions was made mainly based on the inclusion and exclusion of lipid cores. Extracellular vacuoles and lacunae on the Azan-Mallory and HE stained specimens were considered to be lipid cores.

In the ascending-arch and thoracic aortas of WHHLMI rabbits, a total of 191 histopathological features which correspond to the classification criteria were observed (neointimal, n=14; atheromatous, n=44; fibroatheromatous, n=56, and collagen-rich, n=77). There were no lesions showing plaque rupture or thrombi (type VI) in the present study. Thus, the 191 regions were divided into the 4 lesion-categories and semi-quantitatively evaluated in subsequent analyses.

Semi-quantitative Analyses Areas (μm^2) occupied by each lesion component were evaluated with a VHX Digital Microscope (Keyence Corp., Osaka, Japan). The vulnerability index, an index of the morphological destabilized characteristics of atherosclerotic lesions in WHHLMI rabbits, was calculated for each atherosclerotic region as previously described.[24,30] The vulnerability index was defined as the ratio of the lipid component area (macrophages+extracellular lipid deposits)/fibromuscular component area (smooth mus-

cle cells+collagen fibers). Collagen-rich fibers and extracellular lipid deposits (extracellular vacuoles and lacunae) were assessed with Azan-Mallory staining. The macrophage and smooth muscle cell areas were determined with immunohistochemical staining (RAM11 and 1A4). MT1-MMP, MMP-2, and COX-2 staining were assessed as percentages of positively stained areas (% positive).

Statistical Analyses Data are presented as the mean± S.D. Comparisons among lesion types were performed using the Kruskal–Wallis test with *post hoc* analysis by the Scheffe test. Correlation coefficients were assessed with Spearman rank correlation coefficients. Comparisons of correlation coefficients were performed using Fisher's *Z*-transformation. Statistical significance was defined as $p<0.05$.

RESULTS

MT1-MMP, MMP-2 and COX-2 Distribution in Atherosclerotic Lesions Figure 1 shows representative photomicrographs of aortic tissues of the control rabbits. No obvious atherosclerotic changes were observed in the control rabbits.

In the WHHLMI rabbits, various atherosclerotic changes were observed with different staining levels of MT1-MMP, MMP-2, and COX-2. Figure 2 shows typical images of the 4 categories of lesion types with Azan-Mallory, HE and immunohistochemical staining. MT1-MMP staining was prominent in the atheromatous lesions, which were also the regions where macrophages were accumulated (Figs. 2J, R). Weak staining of MT1-MMP was observed in the lipid core regions of fibroatheromatous lesions and superficial regions of collagen-rich lesions, with no obvious staining in the neointimal lesions or medial regions (Figs. 2Q—T). The staining profile of MMP-2 was similar to that of MT1-MMP, except for relatively high staining of MMP-2 in the medial regions (Figs. 2U—X). COX-2 staining was widely observed in the atherosclerotic lesions of the WHHLMI rabbits. Strong COX-2 staining was detected in the macrophage-rich regions of the atheromatous and fibroatheromatous lesions. Weak to moderate COX-2 staining was detected also in the superficial regions of the neointimal and collagen-rich lesions (Figs. 2Y—b).

Highly magnified photomicrographs of immunostaining for the lipid core and medial regions of atheromatous lesions are shown in Fig. 3. MT1-MMP, MMP-2, and COX-2 staining was prominently observed in the lipid core regions colocalizing with macrophage staining (Figs. 3A—D). Relatively strong staining of MMP-2 was observed in the medial regions where smooth muscle actin was positively stained (Figs. 3F, H).

Semi-quantitative Analyses of MT1-MMP, MMP-2 and COX-2 Distribution in Relation to Plaque Vulnerability Figure 4A shows the vulnerability index calculated for each lesion category classified as described in Materials and Methods. This index was the highest in the atheromatous lesions ($p<0.0001$ *vs.* other lesions), followed in decreasing order by the fibroatheromatous lesions ($p<0.005$ *vs.* neointimal lesions; $p<0.0001$ *vs.* collagen-rich lesions), collagen-rich lesions, and neointimal lesions. MT1-MMP staining (% positive) was the highest in the atheromatous lesions, where it was 10.9-, 3.5-, and 6.3-fold higher than that in the neointimal, fibroatheromatous, and collagen-rich lesions, respectively ($p<0.0001$ *vs.* other lesions, Fig. 4B). MMP-2 staining (% positive) was also the highest in the atheromatous lesions among the four lesion types: 4.8-, 2.5-, and 4.2-fold higher than that in the neointimal, fibroatheromatous, and collagen-rich lesions, respectively ($p<0.0001$ *vs.* other lesions, Fig. 4C). The highest staining of COX-2 (% positive) was also found in the atheromatous lesions, while comparable staining levels were observed in the neointimal and fibroatheromatous lesions (Fig. 4D). The % positive area of COX-2 in the atheromatous lesions was 1.2-, 1.3-, and 1.7-fold that in the neointimal, fibroatheromatous, and collagen-rich lesions, respectively (N.S., *vs.* neointimal and fibroatheromatous lesions; $p<0.0001$ *vs.* collagen-rich lesions).

Analyses of Correlations Among MT1-MMP, MMP-2 and COX-2 Staining and Histological Vulnerability Analysis of the correlation of the vulnerability index with MT1-MMP, MMP-2 and COX-2 staining (% positive) is shown in Figs. 5A—C. MT1-MMP staining was positively correlated with the vulnerability index ($r=0.63$, $p<0.0001$, Fig. 5A). Similarly, MMP-2 and COX-2 staining was positively correlated with the vulnerability index ($r=0.60$, $p<0.0001$ for MMP-2; $r=0.36$, $p<0.0001$ for COX-2, Figs. 5B, C). The correlation of the vulnerability index with MT1-MMP and MMP-2 staining was significantly stronger than that with COX-2 staining ($p<0.05$, for each).

Figures 5D—F show the regression analyses among MT1-MMP, MMP-2 and COX-2 staining (% positive). The regression analyses demonstrated positive correlations between MT1-MMP and MMP-2 staining ($r=0.61$, $p<0.0001$, Fig. 5D), between MT1-MMP and COX-2 staining ($r=0.33$, $p<0.0001$, Fig. 5E), and between MMP-2 and COX-2 staining ($r=0.46$, $p<0.0001$, Fig. 5F). The correlation between MT1-MMP and MMP-2 staining was significantly stronger than those between MT1-MMP and COX-2 and between MMP-2 and COX-2 ($p<0.05$, for each).

DISCUSSION

In the present study, we first demonstrated the co-distribution of MT1-MMP, MMP-2, and COX-2 in atherosclerotic lesions. The preferential distribution of these enzymes in the atheromatous lesions (grade IV atheroma) provides *in vivo* evidence for the possible interaction among these enzymes in the destabilization of atherosclerotic plaques. Relatively high COX-2 distribution was also found in other more stable lesions, indicating additional roles of COX-2 in the stabilization of atherosclerotic lesions.

Colocalization of MT1-MMP, MMP-2, and COX-2 in Grade IV Atheroma Recent evidence about the pathophysiology of atherosclerosis suggests that a signaling cascade, namely, activation of pro-MMP-2 to active MMP-2 by MT1-MMP through the PG E_2/cAMP pathway, may play pivotal roles in the destabilization of atherosclerotic plaques. However, there has been no direct evidence regarding the interactions of MT1-MMP, MMP-2, and COX-2 in atherosclerotic lesions. In the present study, we immunohistologically demonstrated the colocalization of MT1-MMP, MMP-2, and COX-2 in the atheromatous lesions (grade IV atheroma) with the highest vulnerability index (Figs. 2 to 4). In addition, these enzymes were prominently localized in the macrophage-rich lipid core region of the grade IV atheroma

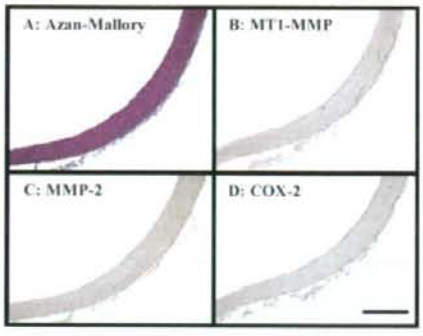

Fig. 1. Photomicrographs of Aortic Tissues of the Control Rabbit

Azan-Mallory staining (A) and immunohistochemical staining for MT1-MMP (B), MMP-2 (C), and COX-2 (D) are shown. Bar=500 μm.

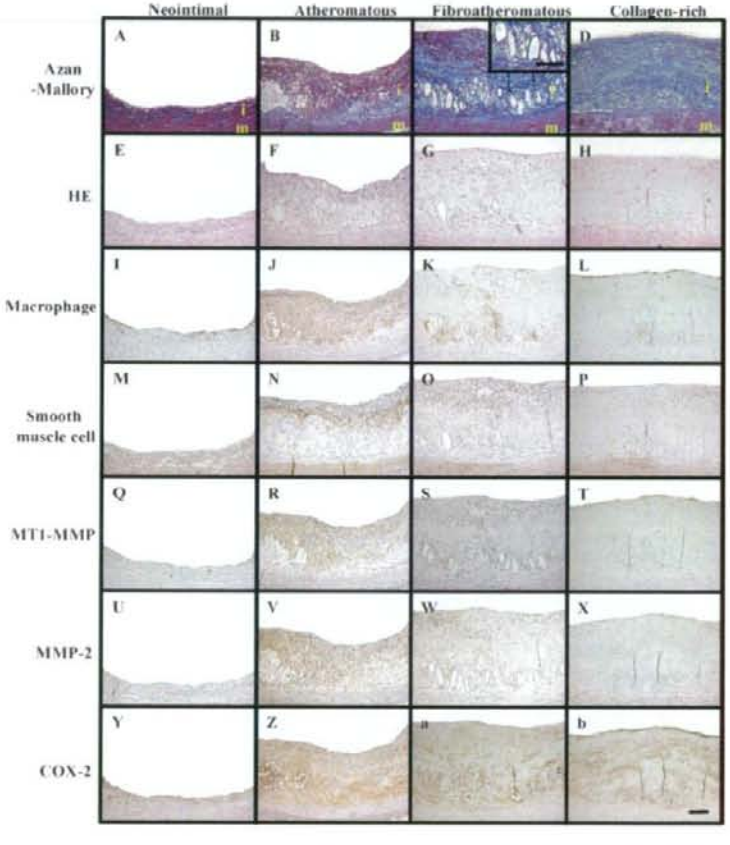

Fig. 2. Typical Photomicrographs of Histological Features of Atherosclerotic Lesions in WHHLMI Rabbits

Atherosclerotic lesions were microscopically divided into 4 categories as described in Materials and Methods: neointimal (left column), atheromatous (middle-left column), fibroatheromatous (middle-right column) and collagen-rich (right column) lesions. Azan-Mallory staining (A to D), HE staining (E to H), and immunostaining for macrophages (I to L), smooth muscle cells (M to P), MT1-MMP (Q to T), MMP-2 (U to X), and COX-2 (Y to b) are shown. A high-magnification photomicrograph of Azan-Mallory staining in the lipid core region is shown in an inset (C). m, media; i, intima; Bar=100 μm.

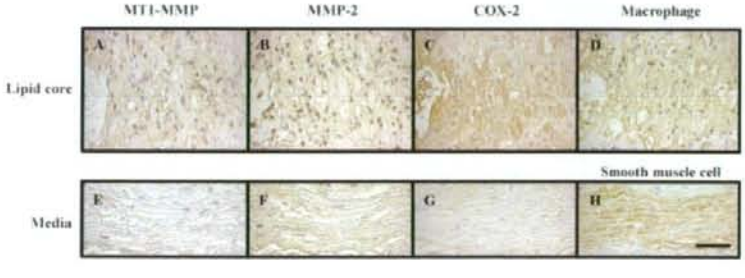

Fig. 3. High-Magnification Photomicrographs of Immunohistochemical Staining for MT1-MMP (A, E), MMP-2 (B, F), COX-2 (C, G), Macrophages (D), and Smooth Muscle Cells (H) in the Lipid Core (A to D) and Medial (E to H) Regions of the Atheromatous Lesions Shown in Fig. 2

Bar=50 μm.

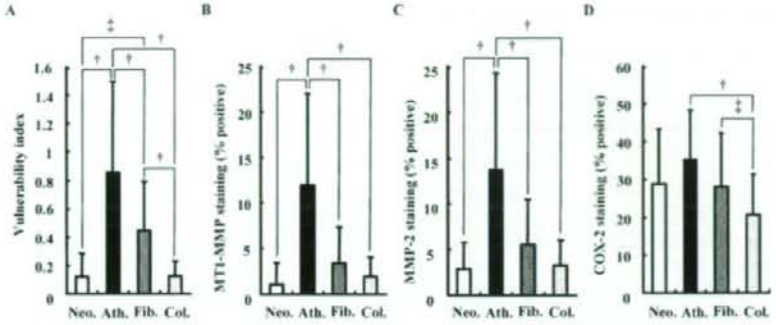

Fig. 4. Vulnerability Index (A) and Percentages of Positively Stained Areas (% Positive) for MT1-MMP (B), MMP-2 (C), and COX-2 (D) in Atherosclerotic Lesions

Neo., Ath., Fib. and Col. indicate neointimal, atheromatous, fibroatheromatous and collagen-rich lesions, respectively. Data are presented as the mean±S.D. Comparisons among lesion types were performed using the Kruskal–Wallis test with *post hoc* analysis by the Scheffe test. †$p<0.0001$, ‡$p<0.05$.

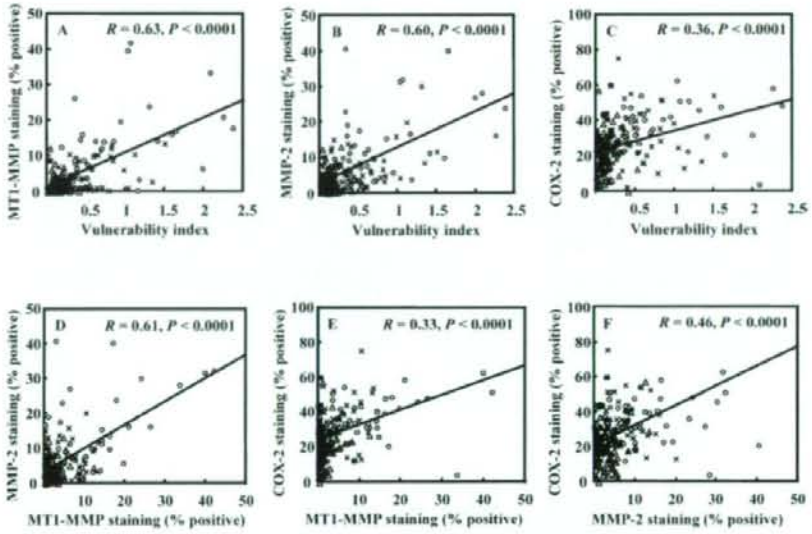

Fig. 5. Analyses of Correlations among MT1-MMP, MMP-2 and COX-2 Staining and Histological Vulnerability

■; neointimal, ○; atheromatous, ×; fibroatheromatous, △; collagen-rich lesions. A—C: Correlations of vulnerability index with MT1-MMP (A), MMP-2 (B), and COX-2 (C) staining (% positive). D—F: Correlations among MT1-MMP, MMP-2 and COX-2 staining (% positive). Correlation coefficients were assessed with Spearman rank correlation coefficients. Comparisons of correlation coefficients were performed using Fisher's *Z*-transformation.

(Figs. 2, 3). These findings support the possibility of interactions among MT1-MMP, MMP-2, and COX-2 and their contribution to plaque progression and rupture.

Distribution of MT1-MMP/MMP-2 In the present study, we investigated MT1-MMP distribution in a rabbit model of atherosclerosis. To the best of our knowledge, this is the first report demonstrating MT1-MMP distribution in atherosclerotic lesions of an animal model. The distribution profiles of MT1-MMP and MMP-2 in our rabbits are mostly consistent with the previous clinical studies that demonstrated a notable colocalization of MT1-MMP and MMP-2 with macrophages in lipid-rich human atherosclerotic plaques.[10,11] In addition, the current results demonstrated that MT1-MMP distribution was positively correlated with vulnerability index and MMP-2 distribution (Fig. 5). Accordingly, our findings further support the contribution of MT1-MMP/MMP-2 to the destabilization of atherosclerotic plaques.[10,11]

It should be noted, however, that dual roles of MMPs have been well documented.[31] MMP activities not only contribute to weakening of the plaque cap *via* cleavage of the ECM but also determine lesion stability through the cleavage of non-matrix substrates, including cytokines, growth factors, and their receptors.[4,8,11] Recently, Kuzuya *et al.* examined the effects of MMP-2 deficiency on atherosclerotic lesion formation in apolipoprotein E-deficient (ApoE−/−) mice.[32] Based on their results, they suggested that MMP-2 may induce plaque stability by promoting the accumulation of SMCs in the fibrous cap, while they showed different effects of MMP-2 on the macrophage accumulation in the atherosclerotic le-

sions of different regions of the artery. Further studies will be required to determine the full spectrum of antiatherogenic or proatherogenic activities of MMPs expressed in atherosclerotic lesions.

In our rabbits, no significant staining of MT1-MMP was found in the medial regions (SMCs) with slight to moderate staining of MMP-2. Contrary to our results, previous clinical studies showed a notable distribution of MT1-MMP and MMP-2 in the media (SMCs) underlying fibrous and lipid-rich regions, suggesting a contribution of MT1-MMP and MMP-2 to SMC-mediated vascular remodeling.[10,11] *In vitro* experiments have also shown that MT1-MMP expression increases not only in macrophages but also in SMCs after proinflammatory stimulation.[10,11,33] Although the reason for the discrepancy remains unclear, differences in species, age, and stage of atherosclerosis may partly explain the discrepancy. Distribution profiles of MMPs may change according to age and stage of atherosclerosis.[4,31] On the other hand, it is reported that MT1-MMP provided by macrophages may play a significant role in the activation of MMP-2 produced by other cells, such as SMCs.[11,14] MMP-2 is constitutively expressed in medial SMCs.[31] These facts may be another explanation for the uncoupling of MT1-MMP and MMP-2 distribution in the medial regions (SMCs).

Distribution of COX-2 in Relation to MT1-MMP Distribution Although there is increasing evidence that COX-2 plays an important role in the pathophysiology of atherosclerotic plaques, the relationship between MT1-MMP and COX-2 has been poorly understood. In particular, there has been no report investigating *in vivo* co-distribution of these enzymes in atherosclerotic lesions, except for one clinical study reported by Hong *et al.*[21] Our present study demonstrated relatively strong staining of MT1-MMP and COX-2 in the macrophage-rich regions of the atheromatous and fibroatheromatous lesions in a rabbit model, which is concordant with the clinical results reported by Hong *et al.* These results are further supported by the previous *in vitro* findings of the enhanced expression of MT1-MMP in human macrophages after proinflammatory stimulation, such as ox-LDL or TNF-α.[11,33] Shankavaram *et al.* also demonstrated that induction of monocyte MT1-MMP is regulated through the PG E_2/cAMP pathway, indicating the important role of COX-2 in the regulation of MT1-MMP.[14] Taken together, these facts imply that MT1-MMP production through the COX-2 dependent pathway may also promote plaque instability, as does the production of other MMPs, including MMP-2 and MMP-9.[12,20]

In our WHHLMI rabbits, relatively strong COX-2 staining was found also in more stable atherosclerotic lesions, such as neointimal and collagen-rich lesions (Figs. 2, 3), indicating that the distribution of COX-2 and MT1-MMP/MMP-2 was uncoupled in these lesions. In addition, the correlation of COX-2 staining with the vulnerability index was significantly weaker compared with those of MT1-MMP and MMP-2 (Fig. 5). This COX-2 distribution profile is in accordance with previous studies where COX-2 distribution was found in early to advanced atherosclerotic lesions in ApoE−/− mice and humans.[18,34] The contribution of COX-2 to early atherosclerotic lesion formation has been suggested.[34] On the other hand, uncoupling between MT1-MMP and COX-2 distribution has not been reported, and the reason for the uncoupling observed here remains unclear. However, it should be noted that COX-2 is only an intermediate enzyme in the metabolic pathway of arachidonic acid, and that the COX-2 bioproduct PGH_2 is further metabolized by other isomerases to various prostanoids. The PG isomerase profile may influence the pro-inflammatory or anti-inflammatory role of COX-2 and may regulate MMP production in atherosclerotic plaques.[15,20] Our findings, namely relatively strong COX-2 staining with weak staining of MT1-MMP in more stable atherosclerotic lesions, appear to support the dual-phase functions of COX-2 reported by Cipollone *et al.*[12,15,20]

Methodological Considerations In the present study, WHHLMI rabbits were used to determine the distribution profiles of MT1-MMP, MMP-2 and COX-2 in comparison with plaque instability analysis, because they have several advantages as an animal model for studying atherosclerosis: (1) lipoprotein profile similar to that of humans, (2) susceptibility to the development of atherosclerosis, (3) lesion characteristics (from early to advanced stage) similar to those in humans.[22,23,35,36] One drawback in our rabbits is that they failed to show any lesion ruptures or thrombosis, although rupture-prone unstable plaques characterized in humans as those consisting of thin fibromuscular caps and large lipid cores with numerous macrophages were observed in the aortic lesions of our rabbits. The atherosclerotic lesions found in the aortas of our rabbits may not exactly follow the process leading to plaque rupture, which may partly explain the discrepancy between the present results and the previous clinical studies. On the other hand, it is reported that plaque rupture was detected in the coronary lesions of WHHLMI rabbits that died by myocardial infarction, although the frequency was rather low.[35] Detail studies in the coronary lesions of WHHLMI rabbits may help clarify the discrepancy between the present results and the previous clinical studies, and provide further important information on the pathophysiology leading to myocardial infarction, as the WHHLI rabbits are the rabbit model of spontaneous myocardial infarction.

The distribution of MT1-MMP, MMP-2, and COX-2 was immunohistologically determined in the atherosclerotic lesions. The immunohistological staining is a useful and widely accepted method for the evaluation of regional distribution of proteins, including enzymes, receptors, and transporters, in human and animal tissues.[6,10–12,18,21] The immunohistological staining, however, can not provide information on the synthesis or degradation of the antigen proteins. In this regard, it is of importance to determine the expression levels of corresponding mRNA. Further elucidation, combined with *in situ* hybridization, is strongly required to determine the dynamic processes of the expression, interaction, and degradation of MT1-MMP, MMP-2, and COX-2. Differential evaluation of pro-MMPs and active-MMPs should also provide useful information regarding the interactions among the enzymes.

CONCLUSION

The present study demonstrated the co-distribution of MT1-MMP, MMP-2, and COX-2 in grade IV atheroma, using hypercholesterolemic rabbits whose pathological characteristics are relevant to human atherosclerosis. These find-

ings support our hypothesis that the activation of pro-MMP-2 to active MMP-2 by MT1-MMP through the PG E_2/cAMP pathway may play pivotal roles in the destabilization of atherosclerotic plaques. In addition, relatively strong COX-2 staining was observed in other more stable lesions, indicating uncoupling between COX-2 and MT1-MMP/MMP-2 distribution. COX-2 may be associated with both the destabilization and stabilization of atherosclerotic lesions *via* its pro- and anti-inflammatory activities. The present findings should help advance our understanding of the pathophysiology of atherosclerosis and provide useful information for the development of new therapeutic and diagnostic (imaging) agents that target MMPs and COX-2 in atherosclerosis.

Acknowledgements This work was partly supported by a Grant-in-Aid for General Scientific Research from the Ministry of Education, Culture, Sports, Science and Technology of Japan, by a Grant-in-Aid for General Scientific Research from the Japan Society for the Promotion of Science, by a research grant from New Energy and Industrial Technology Development Organization (NEDO), and by the 21st Century COE Program 'Knowledge Information Infrastructure for Genome Science'.

REFERENCES

1) Cipollone F., Fazia M., Mezzetti A., *J. Thromb. Haemost.*, **3**, 1962—1975 (2005).
2) Stoll G., Bendszus M., *Stroke*, **37**, 1923—1932 (2006).
3) Jones C. B., Sane D. C., Herrington D. M., *Cardiovasc. Res.*, **59**, 812—823 (2003).
4) Galis Z. S., Khatri J. J., *Circ. Res.*, **90**, 251—262 (2002).
5) Galis Z. S., Sukhova G. K., Lark M. W., Libby P., *J. Clin. Invest.*, **94**, 2493—2503 (1994).
6) Brown D. L., Hibbs M. S., Kearney M., Loushin C., Isner J. M., *Circulation*, **91**, 2125—2131 (1995).
7) Li Z., Li L., Zielke H. R., Cheng L., Xiao R., Crow M. T., Stetler-Stevenson W. G., Froehlich J., Lakatta E. G., *Am. J. Pathol.*, **148**, 121—128 (1996).
8) Visse R., Nagase H., *Circ. Res.*, **92**, 827—839 (2003).
9) Sato H., Takino T., Okada Y., Cao J., Shinagawa A., Yamamoto E., Seiki M., *Nature* (London), **370**, 61—65 (1994).
10) Rajavashisth T. B., Xu X. P., Jovinge S., Meisel S., Xu X. O., Chai N. N., Fishbein M. C., Kaul S., Cercek B., Sharifi B., Shah P. K., *Circulation*, **99**, 3103—3109 (1999).
11) Stawowy P., Meyborg H., Stibenz D., Stawowy N. B. P., Roser M., Thanabalasingam U., Veinot J. P., Chretien M., Seidah N. G., Fleck E., Graf K., *Circulation*, **111**, 2820—2827 (2005).
12) Cipollone F., Prontera C., Pini B., Marini M., Fazia M., De Cesare D., Iezzi A., Ucchino S., Boccoli G., Saba V., Chiarelli F., Cuccurullo F., Mezzetti A., *Circulation*, **104**, 921—927 (2001).
13) Corcoran M. L., Stetler-Stevenson W. G., DeWitt D. L., Wahl L. M., *Arch. Biochem. Biophys.*, **310**, 481—488 (1994).
14) Shankavaram U. T., Lai W. C., Netzel-Arnett S., Mangan P. R., Ardans J. A., Caterina N., Stetler-Stevenson W. G., Birkedal-Hansen H., Wahl L. M., *J. Biol. Chem.*, **276**, 19027—19032 (2001).
15) Cipollone F., Fazia M., Iezzi A., Ciabattoni G., Pini B., Cuccurullo C., Ucchino S., Spigonardo F., De Luca M., Prontera C., Chiarelli F., Cuccurullo F., Mezzetti A., *Arterioscler. Thromb. Vasc. Biol.*, **24**, 1259—1265 (2004).
16) Davies N. M., Good R. L., Roupe K. A., Yanez J. A., *J. Pharm. Pharm. Sci.*, **7**, 217—226 (2004).
17) Matsumoto H., Naraba H., Murakami M., Kudo I., Yamaki K., Ueno A., Oh-ishi S., *Biochem. Biophys. Res. Commun.*, **230**, 110—114 (1997).
18) Baker C. S., Hall R. J., Evans T. J., Pomerance A., Maclouf J., Creminon C., Yacoub M. H., Polak J. M., *Arterioscler. Thromb. Vasc. Biol.*, **19**, 646—655 (1999).
19) Schonbeck U., Sukhova G. K., Graber P., Coulter S., Libby P., *Am. J. Pathol.*, **155**, 1281—1291 (1999).
20) Cipollone F., *Lupus*, **14**, 756—759 (2005).
21) Hong B. K., Kwon H. M., Lee B. K., Kim D., Kim I. J., Kang S. M., Jang Y., Cho S. H., Kim H. K., Jang B. C., Cho S. Y., Kim H. S., Kim M. S., Kwon H. C., Lee N., *Yonsei Med. J.*, **41**, 82—88 (2000).
22) Shiomi M., Ito T., Tsukada T., Yata T., Ueda M., *Arterioscler. Thromb.*, **14**, 931—937 (1994).
23) Shiomi M., Ito T., Yamada S., Kawashima S., Fan J., *Arterioscler. Thromb. Vasc. Biol.*, **23**, 1239—1244 (2003).
24) Ishino S., Kuge Y., Takai N., Tamaki N., Strauss H. W., Blankenberg F. G., Shiomi M., Saji H., *Eur. J. Nucl. Med. Mol. Imaging.*, **34**, 889—899 (2007).
25) Kinoh H., Sato H., Tsunezuka Y., Takino T., Kawashima A., Okada Y., Seiki M., *J. Cell Sci.*, **109**, 953—959 (1996).
26) Tatsuguchi A., Fukuda Y., Ishizaki M., Yamanaka N., *Digestion*, **60**, 246—254 (1999).
27) Stary H. C., Chandler A. B., Glagov S., Guyton J. R., Insull W., Jr., Rosenfeld M. E., Schaffer S. A., Schwartz C. J., Wagner W. D., Wissler R. W., *Circulation*, **89**, 2462—2478 (1994).
28) Stary H. C., Chandler A. B., Dinsmore R. E., Fuster V., Glagov S., Insull W., Jr., Rosenfeld M. E., Schwartz C. J., Wagner W. D., Wissler R. W., *Circulation*, **92**, 1355—1374 (1995).
29) Shiomi M., Ito T., Hirouchi Y., Enomoto M., *Ann. N.Y. Acad. Sci.*, **947**, 419—423 (2001).
30) Shiomi M., Ito T., Hirouchi Y., Enomoto M., *Atherosclerosis*, **157**, 75—84 (2001).
31) Newby A. C., *Physiol. Rev.*, **85**, 1—31 (2005).
32) Kuzuya M., Nakamura K., Sasaki T., Cheng X. W., Itohara S., Iguchi A., *Arterioscler. Thromb. Vasc. Biol.*, **26**, 1120—1125 (2006).
33) Ray B. K., Shakya A., Turk J. R., Apte S. S., Ray A., *Circ. Res.*, **95**, 1082—1090 (2004).
34) Burleigh M. E., Babaev V. R., Oates J. A., Harris R. C., Gautam S., Riendeau D., Marnett L. J., Morrow J. D., Fazio S., Linton M. F., *Circulation*, **105**, 1816—1823 (2002).
35) Shiomi M., Ito T., Yamada S., Kawashima S., Fan J., *J. Atheroscler. Thromb.*, **11**, 184—189 (2004).
36) Liang J., Liu E., Yu Y., Kitajima S., Koike T., Jin Y., Morimoto M., Hatakeyama K., Asada Y., Watanabe T., Sasaguri Y., Watanabe S., Fan J., *Circulation*, **113**, 1993—2001 (2006).

Eur J Nucl Med Mol Imaging (2007) 34:2096–2105
DOI 10.1007/s00259-007-0529-8

ORIGINAL ARTICLE

Extensive FDG uptake and its modification with corticosteroid in a granuloma rat model: an experimental study for differentiating granuloma from tumors

Songji Zhao · Yuji Kuge · Masashi Kohanawa · Toshiyuki Takahashi · Hidekazu Kawashima · Takashi Temma · Toshiki Takei · Yan Zhao · Koh-ichi Seki · Nagara Tamaki

Received: 6 July 2006 / Accepted: 3 July 2007 / Published online: 1 September 2007

Abstract
Introduction Increased ^{18}F-fluorodeoxyglucose (FDG) uptake in inflammatory lesions, particularly in granulomatous inflammation (e.g., sarcoidosis), makes it difficult to differentiate malignant tumors from benign lesions and is the main source of false-positive FDG-PET findings in oncology. Here, we developed a rat granuloma model and examined FDG uptake in the granuloma. The effects of corticosteroid on FDG uptake in the granuloma were compared with those in a malignant tumor.

Methods Rats were inoculated with *Mycobacterium bovis* bacillus Calmette-Guérin (BCG) or allogenic hepatoma cells, and subdivided into control and pretreated (methylprednisolone acetate, 8 mg/kg i.m.) groups. Radioactivity in tissues was determined 1 h after the FDG injection. FDG-PET was performed in rats bearing BCG granulomas or tumors before and after prednisolone treatment.

Results Mature epithelioid cell granuloma-formation and massive lymphocyte-infiltration were observed in the control group of granuloma, histologically similar to sarcoidosis. The mean FDG uptake in the granuloma was comparable to that in the hepatoma. Prednisolone reduced epithelioid cell granuloma-formation and lymphocyte-infiltration. Prednisolone significantly decreased the level of FDG uptake in the granuloma (52% of control), but not in the hepatoma. The FDG uptake levels in the granulomas and tumors were clearly imaged with PET.

Conclusion We developed an intramuscular granuloma rat model that showed a high FDG uptake comparable to that of the tumor. The effect of prednisolone pretreatment on FDG uptake was greater in the granuloma than in the tumor. These results suggest that BCG-induced granuloma may be a valuable model and may provide a biological basis for FDG studies.

Keywords FDG · Granuloma · Tumor · Corticosteroid · Rat

S. Zhao · T. Takei · Y. Zhao · N. Tamaki (✉)
Department of Nuclear Medicine, Graduate School of Medicine, Hokkaido University,
Kita 15 Nishi 7, Kita-ku,
Sapporo 060-8638, Japan
e-mail: natamaki@med.hokudai.ac.jp

Y. Kuge
Department of Molecular Imaging, Graduate School of Medicine, Hokkaido University,
Sapporo, Japan

Y. Kuge · H. Kawashima · T. Temma
Department of Patho-functional Bioanalysis, Graduate School of Pharmaceutical Sciences, Kyoto University,
Kyoto, Japan

M. Kohanawa
Department of Microbiology, Graduate School of Medicine, Hokkaido University,
Sapporo, Japan

T. Takahashi
Department of Pathology, Hokkaido Gastroenterology Hospital,
Sapporo, Japan

K. Seki
Central Institute of Isotope Science, Hokkaido University,
Sapporo, Japan

Introduction

PET using FDG has become a very useful imaging tool not only for detecting and staging malignant tumors but also for monitoring therapy response and for differentiating malignant tumors from benign lesions [1]. These applications are

based on the increased FDG uptake due to enhanced glucose utilization in most tumors. Recent investigations, however, have shown that FDG accumulates not only in malignant tumors but also in various forms of inflammatory lesions, particularly in granulomatous lesions, such as sarcoidosis or active inflammatory processes after chemoradiotherapy [2–4]. Increased FDG uptake in such inflammatory lesions makes it difficult to differentiate malignant tumors from benign lesions and is the main source of false-positive FDG-PET findings in oncology [5]. Thus, it is of great importance to investigate FDG uptake in granulomatous lesions for accurately differentiating malignant and benign lesions by FDG-PET. However, FDG uptake in granulomatous lesions remains unclarified, mainly due to the lack of suitable animal models. To the best of our knowledge, there have been no studies of FDG uptake in experimental granulomatous lesions to date, although increased FDG uptake in inflammatory lesions has been reported in experimental inflammation induced by intramuscular injection of *Staphylococcus aureus* (*S. aureus*) or turpentine oil [5, 6]. Thus, we developed a granuloma rat model.

In the present study, we induced granuloma in the muscle of rats by BCG inoculation and examined FDG uptake in the granuloma in comparison with that in a tumor. In addition, we determined the effect of predonisolone pretreatment on FDG uptake in the granuloma to evaluate whether corticosteroid pretreatment facilitates the differentiation of malignant tumors from benign lesions by FDG -PET.

Materials and methods

Animal studies

All experimental protocols were approved by the Laboratory Animal Care and Use Committee of Hokkaido University. Eight-week-old male Wistar King Aptekman/hok (WKAH) rats (supplied by the Experimental Animal Institute, Graduate School of Medicine, Hokkaido University, Sapporo) were used in all experiments. The *Mycobacterium bovis* bacillus Calmette-Guérin (BCG), Japan strain, was grown on Middlebrook 7H11 agar (Difco Laboratories, Detroit, Mich), suspended in PBS with 0.05% Tween 20, and stocked at −80°C. A 1×10^7 CFU/rat dose of BCG, which was determined in our preliminary experiments, was inoculated into the left calf muscle of rats to induce appropriate sizes and numbers of granulomatous lesions. To produce an experimental tumor, rats were inoculated with a suspension of allogenic hepatoma cells (KDH-8, 1×10^6 cells/rat) into the left calf muscle [7]. Nineteen days after BCG inoculation or 14 days after KDH-8 inoculation, when the BCG-induced granulomatous lesions were 3–8 mm in diameter, or when the KDH-8-induced tumor tissues were 20–30 mm in diameter, the rats were fasted overnight and then randomly divided into two subgroups: prednisolone (PRE)-pretreated and control (untreated) (n=5–6, in each group). The sizes of the granuloma and tumors were checked under palpation, and then measured using calipers. The rats in the PRE-pretreated group were intramuscularly injected with methylprednisolone acetate (8 mg/kg body weight) in the left brachialis muscle 20 h before the FDG injection, according to the methods reported by Gemma et al. [8]. Each rat was anaesthetized with pentobarbital (50 mg/kg body weight, i.p.) and was injected in the tail vein with 5–6 MBq of FDG. The rats were kept under anaesthesia for the rest of the experiment. Sixty minutes after the FDG injection, the animals were sacrificed and tumor, granuloma tissues, and other organs were excised. The tissues and blood samples were weighed, and radioactivity was determined using a gamma counter (1480 WIZARDTM3″; Wallac Co., Ltd.). FDG uptake in the tissues was expressed as the percentage of injected dose per gram of tissue after being normalized to the animal's weight (%ID/g × kg). The lesion (granuloma or tumor)-to-muscle (L/M) ratio and the lesion (granuloma or tumor)-to-blood (L/B) ratio of FDG uptake were calculated from the (%ID/g)×kg value of each tissue [6]. By using tissue samples from the tumors and granulomas, frozen specimens and formalin-fixed, paraffin-embedded specimens were prepared for subsequent histologic staining. Blood samples for glucose measurement were obtained immediately before FDG injection and immediately before sacrifice. Blood glucose level was determined using a biochemical analyzer (MediSense, Dainobot Co., Ltd.).

Histochemical studies

Immunohistochemical staining for immune-associated antigen (Ia) was performed using a monoclonal antibody (mAb) (mouse IgG, MRC OX-6, Oxford Biotechnology Ltd.) that recognizes a monomorphic determinant of the rat Ia, MHC class II present on B lymphocytes, dendritic cells, some macrophages, and certain ephithelial cells. To further support the Ia-positive (Ia+) staining, other mAbs, namely, MRC OX-3 and MRC OX-17 were also used. The MRC OX-3 mAb (Serotec), a mouse anti-rat RT1Bu mAb, recognizes a polymorphic determinant of the rat Ia-A antigen RT1Bu (class II polymorphic) found on B cells, dendritic cells, and certain epithelial cells. The MRC OX-17 mAb (Serotec) recognizes a monomorphic determinant of the rat RT-1D (class II monomorphic), the rat homologue of the mouse Ia-E, which has a similar structure to the Ia-A antigen and reacts with anti-Ia alloantibodies. The MRC OX-17 mAb does not cross-react with the rat Ia-A (RT-1B) antigen, while both class II monomorphic MRC OX-6 and MRC OX-17 mAbs were active against determinants found in all rat strains. The different cell types were characterized